Materials Science and Engineering R 70 (2010) 151–168

Contents lists available at ScienceDirect

Materials Science and Engineering R

journal homepage: www.elsevier.com/locate/mser

Trends in semiconductor defect engineering at the nanoscale

Edmund G. Seebauer *, Kyong Wook Noh

Department of Chemical and Biomolecular Engineering, University of Illinois at Urbana-Champaign, 600 S. Mathews Ave., Urbana, IL 61801, United States

ARTICLE INFO

Keywords:
Semiconductors
Defect engineering
Defects
Metal oxides
Nanoelectronics

ABSTRACT

Defect engineering involves manipulating the type, concentration, spatial distribution, or mobility of defects within a crystalline solid. Defect engineering in semiconductors has become much more sophisticated in recent years, driven by the need to control material properties at small length scales. The present article describes recent trends in defect engineering across several nano-oriented applications, beginning with Si-based integrated circuits and extending into non-Si microelectronics and especially into oxide semiconductors for sensors and photocatalysis. Special focus fixes upon physical mechanisms that have been little exploited up to now, but show significant promise as new means for controlling defect behavior, including low-energy ion bombardment, surface chemistry, and photostimulation. Systems-based methods for parameter estimation offer considerable promise for helping to understand the complex diffusion and reaction networks that characterize defect behavior in most prospective applications.

Contents

1. Introduction

The technologically useful properties of a semiconductor often depend upon the types and concentrations of the defects it contains. For example, defects mediate dopant diffusion in semiconductors used for microelectronic devices [1–5] in ways that are vital for device fabrication. Defects also affect the performance of semiconductor-based sensors [6], catalysts [7,8], photoactive devices [9–11], and photovoltaic (PV) cells [12]. Defect engineering involves manipulating the type, concentration, spatial distribution, or mobility of defects within the solid. Example methods for achieving such control include specially designed heating protocols (time, maximum temperature, heating and cooling rates), introduction of foreign atoms, specially designed ion

* Corresponding author. Tel.: +1 217 244 9214; fax: +1 217 333 5052.
E-mail address: eseebaue@illinois.edu (E.G. Seebauer).

0927-796X/$ – see front matter © 2010 Elsevier B.V. All rights reserved.
doi:10.1016/j.mser.2010.06.007

bombardment protocols, and amorphization/recrystallization. More recent methods include photostimulation and controlling the chemical state of the surface.

Defect engineering has found the most widespread and sophisticated usage for fabrication of microelectronic devices, whose critical dimensions are now typically in the nanoscale range. This usage has been driven by the need for exquisite control of charge carrier type and concentration, as well as electrical current flow. This literature for Si-based devices has been reviewed extensively [13–16] and some of those reviews incorporate recent trends [17,18]. Several treatments exist for individual defect engineering methods, which constellate around the applications of large-area Si wafer fabrication from the melt, and the subsequent formation of *pn* junctions in field-effect transistors. Large-area Si wafers are fabricated via Czochralski growth, which is capable of producing near-perfect, high-purity substrates. Nevertheless, harmful defects can form during growth, and vigorous efforts have been made to control them [19–21]. Defect engineering methods for *pn* junctions focus upon either ion implantation or the subsequent annealing steps. In addition to general treatments of ion implantation [22–24], there exist extensive discussions of the related methods of co-implantation [25], plasma doping [26–28], and vacancy engineering [29,30]. On the annealing side, most discussions of defect engineering focus upon rapid thermal processing [31–33], or its more recent variant millisecond annealing [33–35].

The use of defect engineering outside of Si-based microelectronics is less extensive, but has still drawn attention in the review literature. For example, several articles exist that treat ion implantation in III–V compound semiconductors for device applications [36–38] or metal oxide nanoparticles for photocatalysts [39,40]. For metal oxides, the broader notion of defect engineering apart from ion implantation is relatively new, and only a few reviews can be found [41,42].

The present article seeks to present an integrated treatment of recent trends in defect engineering across these applications with a focus on the nanoscale, beginning with Si-based microelectronics and extending into non-Si microelectronics and especially into oxide semiconductors in sensors and photocatalysis. Special focus fixes upon physical mechanisms that have been little exploited up to now, but show significant promise as new means for controlling defect behavior.

Table 1
Correspondence in defect structure and behavior for the bulk and surface.

Bulk	Surface
Interstitial atom	Adatom or surface interstitial
Vacancy	Vacancy
Interstitial cluster	Adatom island
Vacancy cluster	Vacancy island
Kick-in/kick-out	Exchange diffusion
Vacancy-interstitial formation	Vacancy-adatom formation

2. Defect characteristics

As a prelude to the discussion of defect engineering, a brief review of the salient defect characteristics will prove useful. Fig. 1 shows how crystalline semiconductors may contain a variety of imperfections involving single atoms (point defects) or multiple atoms (extended defects). Examples of point defects include missing atoms (vacancies), extra atoms wedged between lattice atoms (interstitials), and impurity atoms on lattice sites (substitutionals or dopants). Examples of extended defects include linear or planar mismatches in the lattice (dislocations or stacking faults), clusters of point defects, and grain boundaries. Extended defects are especially prone to form at the interface between two dissimilar semiconductors with different lattice constants. In epitaxial growth applications, the drive to relieve strain induced by the mismatch sometimes leads to threading dislocations that propagate throughout the growing layer.

A free surface (or an interface with a dissimilar material) can be conceptualized as a very large extended defect in the bulk structure. Yet the surface or interface also exhibits two-dimensional regularity in its structure, with defect forms analogous to those found in the bulk [43]. The terminology often differs, however. For example, the surface science community refers to "surface interstitials" as "adatoms." A large agglomeration of vacancy defects in the bulk is a "vacancy cluster"; the analogous feature on the surface is often called a "vacancy island." Table 1 summarizes the correspondences in defect structure and behavior for the bulk and surface. Understanding surface defects is becoming increasingly important in applications – for example, as electronic devices shrink closer to the atomic scale (with the attendant increase in surface-to-volume ratios), and as molecular-level control of catalytic reactions becomes

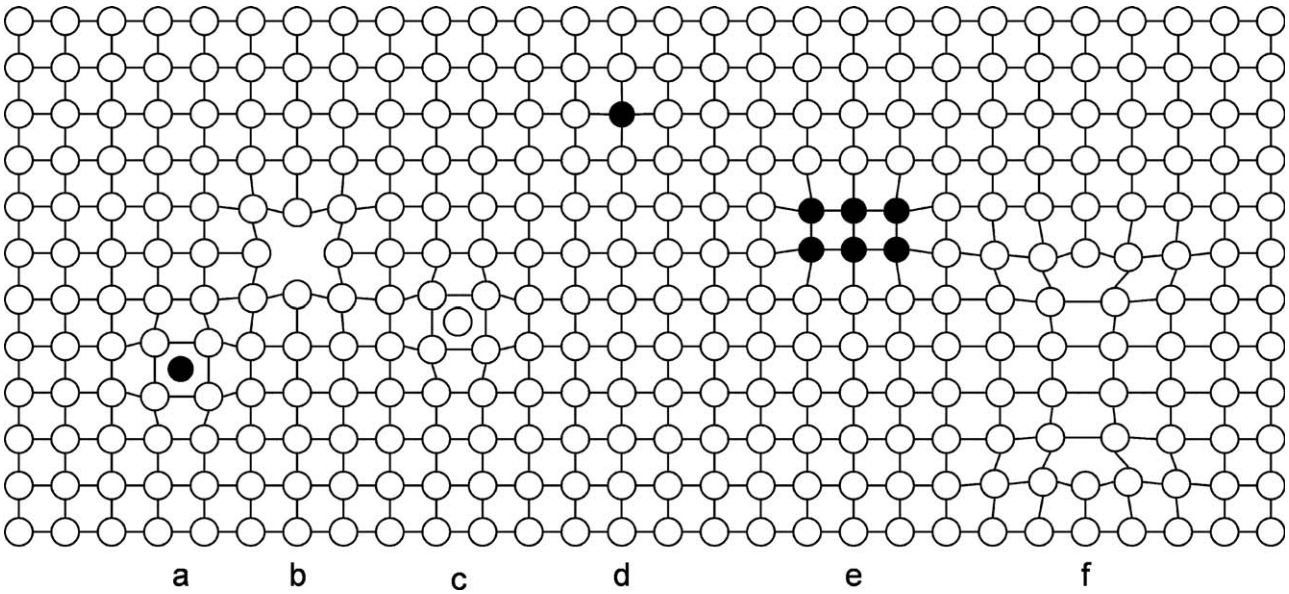

Fig. 1. Examples of common defects in semiconductors: (a) interstitial impurity atom, (b) vacancy, (c) self-interstitial atom, (d) substitutional impurity atom (dopant), (e) precipitate of impurity atoms (cluster), (f) vacancy cluster.

increasingly feasible. The present work will treat surfaces mainly in connection with bulk defects, however.

Defect formation affects semiconductor properties in a variety of ways. Point defects typically affect electronic properties such as carrier type, concentration or mobility [44,45]. Extended defects also affect physical properties, such as strength or toughness [46]. At elevated temperatures, extended defects frequently serve as sources or sinks of point defects. Surfaces do the same, interacting through both bond-exchange [47,48] and electrostatic [47] mechanisms. Most defects can act as sites where electrons and holes recombine with special efficiency [49–51], typically degrading the performance of the host material in applications ranging from optoelectronics to photocatalysis. Defect engineering seeks to reduce such effects.

It has long been known that bulk defects in semiconductors can be electrically charged. Charging of surface defects has been identified and studied more recently. In either case, this charging can affect defect structure [52,53], thermal diffusion rates [54–56], trapping rates of electrons and holes [57,58], and luminescence quenching rates [59]. More interestingly, defect charging also introduces new phenomena such as nonthermally photostimulated diffusion [60–62]. Such phenomena offer completely new mechanisms for defect engineering, as well as new means to study the charging phenomenon itself.

3. Si-based microelectronics

Critical dimensions in Si-based integrated circuits have scaled down well into the range of a few tens of nanometers. Defect engineering in these applications focuses upon the initial creation of Si wafers by Czochralski growth, or upon the later fabrication of *pn* junctions in field-effect transistors (FETs) by ion implantation and annealing.

3.1. Czochralski growth

Highly scaled microelectronic devices require Si wafer substrates that are exceptionally free of defects and impurities. Czochralski growth from the semiconductor melt is the most common manufacturing technique for producing such Si, and extensive efforts have been made to minimize defect formation or incorporation during the growth process. The most common defects that bedevil the grown material are microdefects such as aggregates of vacancies, self-interstitials and oxygen impurities. The resulting defects are often large enough to observe directly via light scattering or transmission electron microscopy (TEM) [20,21]. Yet these defects form by accretion of smaller point defects, which remain largely invisible yet still require control.

Early attempts at defect control were empirical methods involving specialized protocols for heat removal and crystal pulling from the melt to maintain spatial uniformity in temperature [20,63]. Oxygen dissolution within the Si was mitigated through crucible design. Such empiricism led to significant improvements. In recent years, however, detailed mathematical modeling of defect behavior within the high-temperature solid has augmented the experiments. The modeling of defect diffusion, reactions and equilibrium provides useful insights, reduces the number of experiments required to understand defect behavior, and has found direct connection to optimizing commercial processes [19,20,64,65].

For example, modeling coupled with experiments has shown that the majority defect that forms during growth depends upon the ratio of the pull rate v and the temperature gradient G [20,64,65]. At higher v/G ratios, vacancies dominate. Self-interstitials dominate at lower ratios. Recent models incorporate the effects of oxygen on the behaviors of intrinsic defects [66,67], and have extended to more complicated systems where intentional dopants such as nitrogen [67–69] and germanium [70,71] are introduced. The same basic approach has also been applied to growth of germanium and metal oxide crystals [19,21,72].

3.2. Ion implantation for doping

Ion implantation has long been employed to introduce dopants as substitutional defects within the Si lattice [22–24]. As the feature size of devices has shrunk, *pn* junctions in field-effect transistors have become shallower – 20 nm or less from the surface in the source-drain extension regions. The simplest approach to obtaining such shallow junctions has been to reduce the ion energy of the irradiating beam. This approach has notable limits, however. The relative degree of energy spread around the mean ion energy becomes more pronounced at lower energies. Space charge effects within the irradiating beam causes the beam to expand and the ion flux to decrease. Furthermore, channeling of dopant atoms parallel to certain crystal planes becomes more problematic, leading to placement of unwanted dopants deeper than the junction, as well as undesired lattice damage effects. The problems are most pronounced for the *p*-type dopant boron. Plasma based implantation helps to avoid some of these problems as it enables ultra-low-energy implantation at a high beam current, which greatly improves production throughput while keeping the ion penetration depth low [26–28]. In addition, the plasma sheath drives implantation perpendicular to the surface, which is especially useful in three-dimensional structures with large aspect ratios that are difficult to dope using conventional beams [73,74]. For planar structures, however, beamline implantation has retained its ascendancy, and defect engineering techniques have focused on that mode of dopant introduction.

Molecular (or cluster) doping [17,75] represents a method to reduce such implant-related problems. This approach employs molecules or clusters that contain the dopant atoms instead of single ions or small molecular fragments. The large size of the molecule or cluster permits the use of high acceleration voltages, yet the energy per dopant atom remains small. One important consequence is higher fluxes and therefore higher throughput. Also, upon impact with the solid, defect formation is confined to the near-surface region, and channeling is reduced compared to single atoms or small fragments. Early attempts at molecular doping used decaborane ($B_{10}H_{14}$) [76–79], but limitations in source stability and delivery systems retarded development of the technology. Improvements in the source and the use of other molecules such as octadecaborane ($B_{18}H_{22}$) [80–82] and carborane ($C_2B_{10}H_{12}$) [83,84] have reignited interest, however. Junctions with depths less than 10 nm have been successfully fabricated with favorable device characteristics (Fig. 2).

Co-implantation of species in addition to the desired dopant represents another promising method for achieving shallow junctions, although in this case, the focus is on enhancing the dopant's electrical activation and reducing its unwanted diffusion during the annealing step. Again, these issues are most pronounced when boron is the dopant. Early co-implantation work examined the effects of F resulting from the implantation of BF_2. Ohyu et al. [85] examined the efforts of implanting F subsequent to B, and discovered that the diffusion of B upon annealing decreased, and the degree of electrical activation increased. After further demonstration of salutary effects [86], much effort has been expended to determine the mechanism by which F operates [87–92]. The consensus is that F decreases unwanted boron diffusion by reducing the concentration of excess Si interstitials [89,90] that appear during annealing and mediate B diffusion. This effect generally enhances electrical activation as well, although the results are complicated; F occasionally acts to reduce B activation

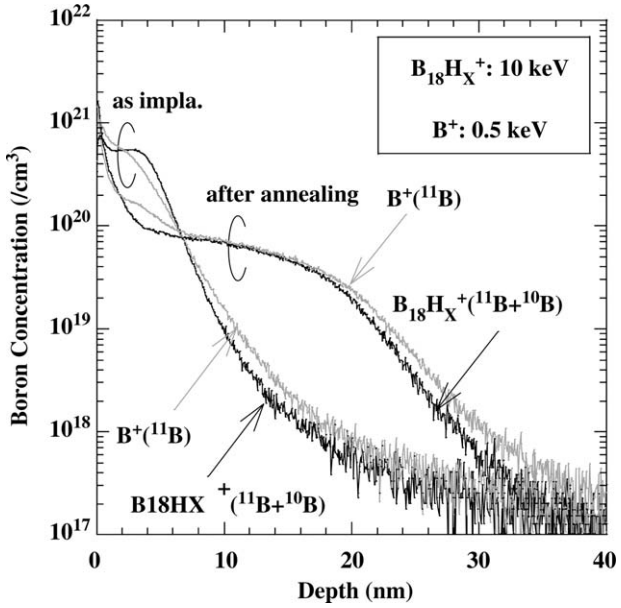

Fig. 2. Secondary ion mass spectroscopy (SIMS) profiles of boron in silicon, before and after annealing of $B_{18}H_x^+$ at 10 keV and B^+ at 0.5 keV. Reproduced from [81].

[87,89,92]. Co-implantation of species other than F has also yielded good results. For example, carbon works well for reducing diffusion [93,94] and increasing activation [95,96] (Fig. 3), either alone or in tandem with F. The operational mechanism again results from a reduction in the concentration of Si interstitials during annealing. Related improvements have been found for the *n*-type dopant phosphorous [97,98]. Nitrogen co-implantation offers benefits similar to C or F in the case of boron doping [99–101]. Indeed, some work is now employing "cocktails" of various co-implantation species [96].

A more subtle and less-investigated mechanism for defect engineering via implantation involves the adjustment of the semiconductor temperature during ion exposure. Such phenomena have been well studied in the context of plasma etching [102–104], ion implantation [105–107], and beam-assisted deposition [108]. Higher temperatures during implantation are known to enhance self-healing and other thermally stimulated processes, rather than the ion-solid interactions themselves. However, measurements of beam-assisted deposition [109–113] and surface diffusion [114,115] have hinted that temperature may directly affect the dynamics of defect formation when ion energies fall below about 100 eV. None of the experiments yielded a conclusive explanation. However, recent molecular dynamics simulations [116,117] and experiments [117,118] show that the threshold energies E_{Thres} at which ions begin to induce sputtering, surface adatom formation, surface atom knock-in, and bulk vacancy formation decrease strongly (>0.1 eV/K) as temperature increases. The threshold energies for these four processes differ from one another, but all obey the following phenomenological relation:

$$E_{Thres} = E_{Tot} - \sigma kT, \tag{1}$$

where E_{Tot} and σ denote constants and k is Boltzmann's constant. Fig. 4 shows an example for surface adatom formation. Most relevant to defect engineering in the bulk, however, is bulk vacancy formation in the vicinity of the surface. In this case, the constants determined by simulation for Si are σ = 700 and E_{Tot} = 92 eV, with the effects being essentially independent of the bombarding ion's mass. For Ge, σ remains the same as for Si, but E_{Tot} decreases in the ratio $E_{Tot,Si}/E_{Tot,Ge}$ = 1.37. This ratio falls close to the ratio of cohesive energies $E_{coh,Si}/E_{coh,Ge}$ = 1.20 and the ratio of melting temperatures $T_{melt,Si}/T_{melt,Ge}$ = 1.40. Such effects are notable because in ion implantation, the final stages of ion deceleration determine the dynamics of defect formation near the *pn* junction [119,120]. Changing the temperature during implantation could controllably modulate such effects. Moreover, the mechanism outlined here is not specific to Group IV semiconductors, and may characterize low-energy ion interactions with crystalline materials quite generally. It may therefore be possible to exploit the threshold effects described here by judicious tuning of temperature and ion energy to select for specific defect formation processes.

3.3. Vacancy engineering

Vacancy engineering is an implantation-based method that in certain respects resembles co-implantation. Vacancy engineering involves the creation of excess vacancies in the doping region via high-energy co-implantation [121]. The core idea is that doping normally creates a supersaturation of Si interstitials that induce

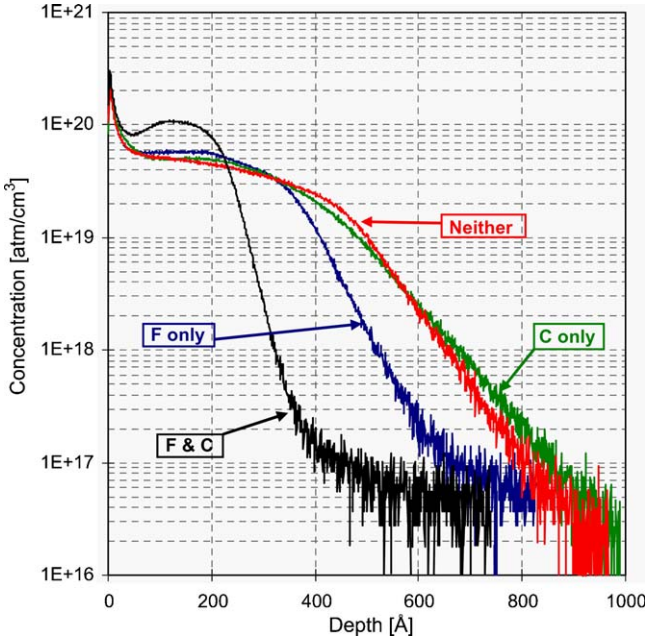

Fig. 3. Annealed boron secondary ion mass spectroscopy (SIMS) profiles of B in Si after annealing with the co-implant conditions labeled. Note the dramatic boron diffusion reduction in the case where F and C co-implants are present. Reproduced from [96].

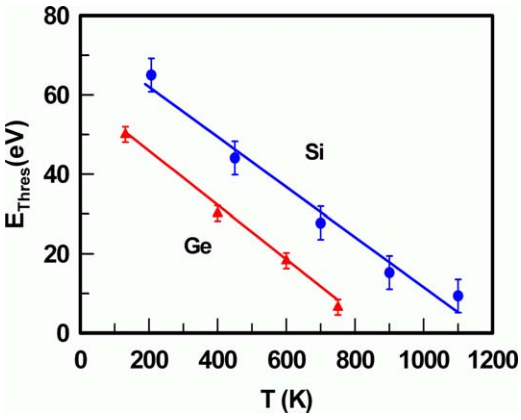

Fig. 4. Dependence of threshold energy upon temperature for Si and Ge adatom formation bombarded with Ar ions, derived from molecular dynamics simulations. Dependence is strong (0.06 eV/K) and obeys the relation $E_{Thres} + \sigma kT = E_{Tot}$ where σ and E_{Tot} are constants.

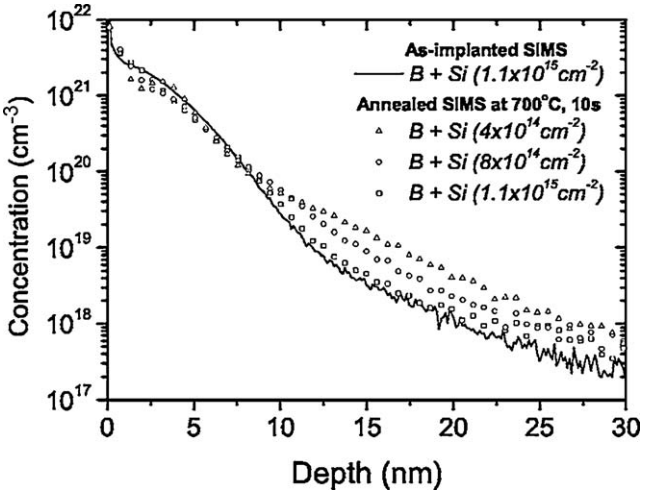

Fig. 5. Secondary ion mass spectroscopy (SIMS) analysis of 500 eV B implants after silicon co-implantation, before and after annealing. Symbols show data for three co-implant doses: 4×10^{14} cm^{-2} (△), 8×10^{14} cm^{-2} (○), and 1.1×10^{15} cm^{-2} (□), after annealing at 700 °C for 10 s. The solid line shows the as-implanted profile (taken from the sample implanted with 1.1×10^{15} cm^{-2} silicon). Reprinted with permission from [126], copyright 2006 American Institute of Physics.

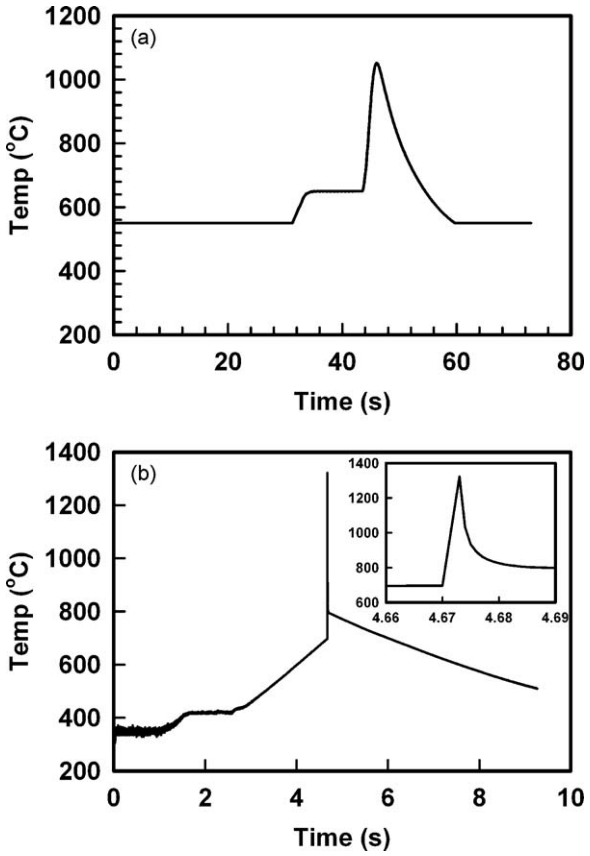

Fig. 6. (a) Temperature trajectory for rapid thermal annealing with a peak temperature of 1050 °C. (b) Annealing program for millisecond anneal experiment with a peak temperature of 1322 °C. Inset shows the detailed temperature trajectory. After [134].

unwanted diffusion [120,122] and electrical deactivation [123,124] of the dopant. Creating excess vacancies can annihilate these interstitials, thus mitigating these problems. The vacancies are generated by a high-energy (MeV) co-implantation of silicon prior to dopant implantation. The high-energy step knocks Si lattice atoms deep into the bulk, leaving excess vacancies in the near-surface region to be implanted. This method eliminates complications resulting from the co-implantation of distinct elements such as N, C or F. The high-energy ions also damage the gate electrode and dielectric. Nevertheless, recent work (Fig. 5) has demonstrated results for boron diffusion and activation that exceed those for conventional implantation in silicon-on-insulator structures [125,126]. There have been promising results for standard bulk silicon substrates as well [127].

3.4. Heating protocols

Annealing is performed after ion implantation in order to heal residual damage and to place dopant atoms substitutionally on lattice sites, thereby making the dopants electrically active. However, heating that provides sufficient atomic mobility to move atoms into substitutional sites can also promote unwanted spreading of the implanted dopant profile. This spreading deepens the *pn* junction undesirably. Over the years, empirical studies demonstrated the significant advantages of heating to increasingly high temperatures for increasingly brief periods. Such protocols tend to reduce diffusional profile spreading and improve electrical activation, and have been termed "rapid thermal annealing" [75]. In practice, such protocols were initially implemented with incandescent lamps to achieve ramp rates up to several hundred K/s, with the time at maximum temperature being on the order of 1 s.

As device sizes scaled downward and junction depths became shallower (20 nm and below in present technology), the trend toward higher temperatures and shorter times continued – to within roughly 100 °C of the melting point of Si for millisecond durations (Fig. 6) [128]. Optical sources have progressed to excimer lasers [129–131], xenon flash lamps [35,129,132,133], and others. Computational modeling has shown [134,135] that short-time annealing constitutes a form of defect engineering. Short times reduce unwanted dopant spreading by greatly reducing the time for diffusion, which more than compensates for an increased concentration of Si interstitials that promote dopant spreading. In moving from conventional rapid thermal annealing to millisecond annealing of boron in Si, for example, the rate of interstitial-mediated dopant diffusion increases by almost 2 orders of magnitude due to the higher temperature, but the time scale is reduced by almost 3 orders of magnitude [136]. The net consequence is reduced profile spreading, as shown in Fig. 7. Millisecond techniques also favorably alter the relative balance of dopant interstitial sequestration by the crystal lattice vs. interstitial clusters, which leads to improved electrical activation at depths just short of the junction. Again, the key factor is the reduction in time scale, which significantly reduces the amount of re-accretion of dopant interstitials into interstitial clusters.

Proper device functioning requires the management of several kinds of defects during processing, ranging from native and dopant point defects to native and dopant defect clusters to extended structures such as end-of-range defects. Consequently, various combinations of millisecond annealing with more conventional thermal annealing have been developed [137,138]. With respect to interstitial clusters, for example, the rate of dissociation depends upon both peak temperature and ramp-rate. A higher ramp-rate reduces cluster dissociation, which keeps dopant atoms locked in an inactive state [132,139,140]. Annealing to higher temperatures can mitigate this problem to some extent. However, differential thermal expansion among the various materials present in the device can lead to wafer warpage or breakage. The melting point of the underlying Si also imposes an obvious constraint. Thus, elevating the annealing temperature suffers limits in terms of dopant activation; removal of end-of-range defects suffers

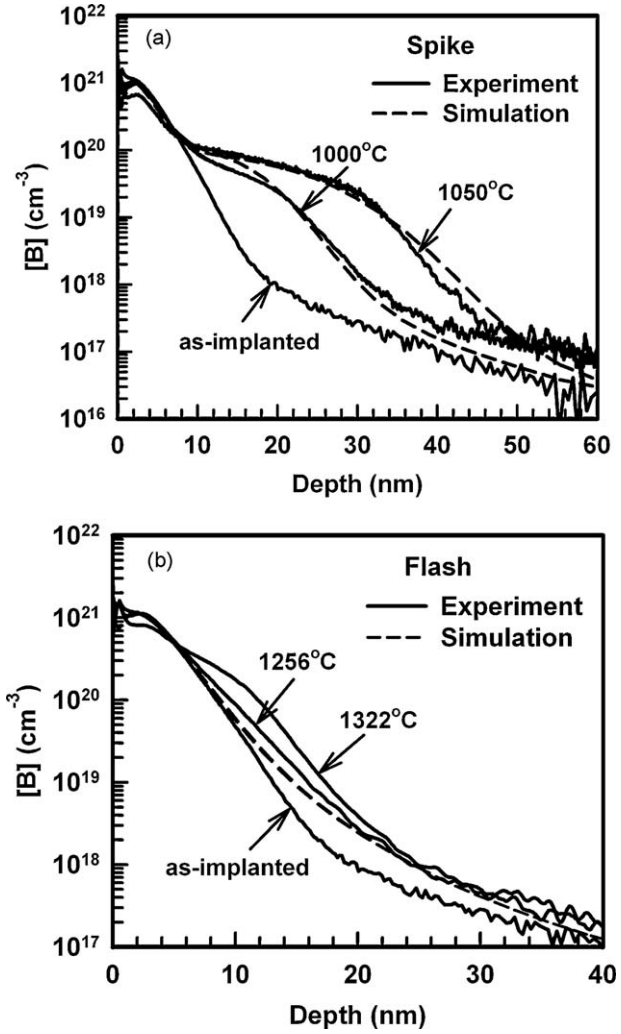

Fig. 7. Experimental and simulated boron profiles in silicon using *a priori* parameter estimates for (a) conventional rapid thermal annealing at 1000 °C and 1050 °C and (b) millisecond annealing to 1256 °C and 1322 °C. The millisecond annealing simulations essentially overlay each other and are indistinguishable from each other, in contrast to the experimental profiles. After [134].

similarly [139,141,142]. Multiple exposures to the optical source (laser beam [142] or flashlamp [143,144]) are sometimes employed to circumvent these problems. Combination of millisecond processing with furnace annealing [137] or conventional rapid thermal annealing [145,146] seeks to accomplish similar goals. However, the optimal combination of laser (or flashlamp) pulse duration, number of pulses, and incorporation of standard annealing methods remains a subject of active research [147].

3.5. Solid phase epitaxial regrowth

Solid phase epitaxial regrowth (SPER) represents a strategy to avoid the strong variations of dopant concentration with depth that ion implantation entails, and to obtain concentrations of active dopant that are larger than the solid solubility limit. In SPER, a surface layer is intentionally amorphized by high-dose ion implantation. Upon heating, recrystallization commences with the underlying crystalline substrate serving as the seed. Dopant atoms diffuse quickly within the amorphous layer, and therefore redistribute themselves fairly uniformly before being frozen in place by recrystallization. Problems with defects remain, however. Large numbers of "end of range" extended defects persist at the original boundary between the amorphous layer and the underlying crystalline seed. These defects promote unwanted current leakage in the finished devices, and also serve as a major source of self-interstitials during subsequent processing steps. The self-interstitials interact with active dopant on lattice sites and deactivate much of it [17,92]. However, extensive modeling of SPER continues by molecular dynamics and atomistic studies to determine the extent to which such problems can be avoided [148–152].

3.6. Surface effects

As junctions move progressively closer to nearby surfaces and interfaces, the possibility arises for using these boundaries themselves for defect engineering. Such engineering could also prove useful in the formation of three-dimensional devices such as FinFETs, as well as a much wider variety of nanostructures having high surface-to-volume ratios. For example, Jie et al. [153] have recently found that the surface chemical state of Si nanowires affects their electrical properties during operation. Carrier mobility was higher when nanowire field-effect transistors operated in vacuum environments as opposed to air. The performance was further improved when the nanowires were embedded in SiO_2, which passivates the surface defects. Cui et al. [154] used 4-nitrophenyl octadecanoate to passivate the surface defects on the SiO_x coating around Si nanowires, leading to increases in the average transconductance and mobility.

Related effects are being exploited during device processing. For example, it has been shown [17,48,155] that the behavior of point defects within silicon can be engineered by controlling the chemical state at the surface. One mechanism involves exchange of bulk defects into and out of dangling bonds at a surface or interface. An atomically clean surface is chemically active and can annihilate interstitial atoms (when the bulk is supersaturated with them) by simple addition of the interstitials to dangling bonds. However, if the same surface becomes saturated with a strongly bonded adsorbate, annihilation requires the insertion of interstitials into existing bonds. Such insertion should have a higher activation barrier, and the surface becomes less chemically active toward defects. By principles of microscopic reversibility and detailed balance, dangling bond sites should be especially effective

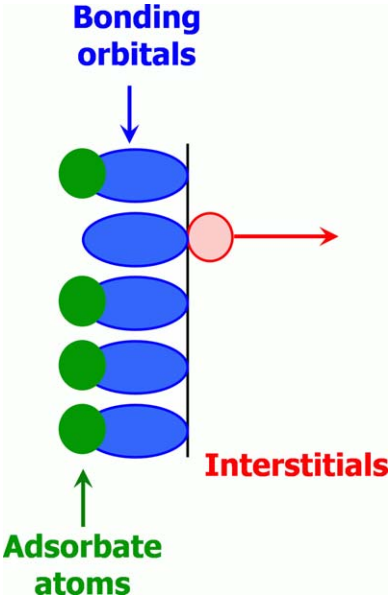

Fig. 8. Schematic diagram indicating how formation of bulk defects (interstitials in this example) is more facile at dangling bond locations at a surface or interface than at locations where the surface or interface bonds are chemically saturated.

at releasing vacancies or interstitials into the bulk if the bulk is undersaturated in those defects. Fig. 8 depicts this phenomenon.

In the specific application of annealing after ion implantation, excess Si interstitials promote the expulsion of dopant atoms from the desired substitutional atomic sites and the unwanted diffusion of those atoms. Annealing protocols that avoid these problems also leave most of the dopant locked within clusters, rendering it useless. The presence of a large nearby surface "sink" solves this problem by removing Si interstitials selectively over dopant interstitials. Dopant interstitials are impeded in their motion to the surface by exchange with the bulk lattice atoms in a way that Si interstitials are not. The reason is statistical. A dopant interstitial diffusing toward the surface periodically kicks into the lattice, and becomes immobile and electrically active. The kick-in process almost always releases an interstitial of the majority species in the lattice (Si), and the immobilized dopant atom must wait for another Si interstitial to come along in order to become mobile again. Silicon interstitials also exchange with the lattice, but at typical doping levels a lattice exchange event simply yields another Si interstitial atom. Thus, the lattice does not impede the net motion of Si interstitials nearly as much as for the dopant.

Recent experiments have demonstrated these effects [48,155–157] via bulk diffusion measurements. For example, a nearby surface that is atomically clean greatly inhibits the self-diffusion of implanted isotopically labeled Si [48]. Controlled adsorption of atomic nitrogen on Si(1 0 0) to saturate dangling bonds has proven capable of controlling the annihilation probability of self-interstitials over two orders of magnitude (Fig. 9), with effects evident even at coverages as small as 0.01 monolayers. Related effects have also been measured for dopants such as arsenic [155] and boron [156]. In the boron case (Fig. 10), the atomically clean, chemically active surface yielded reduced diffusion and increased dopant

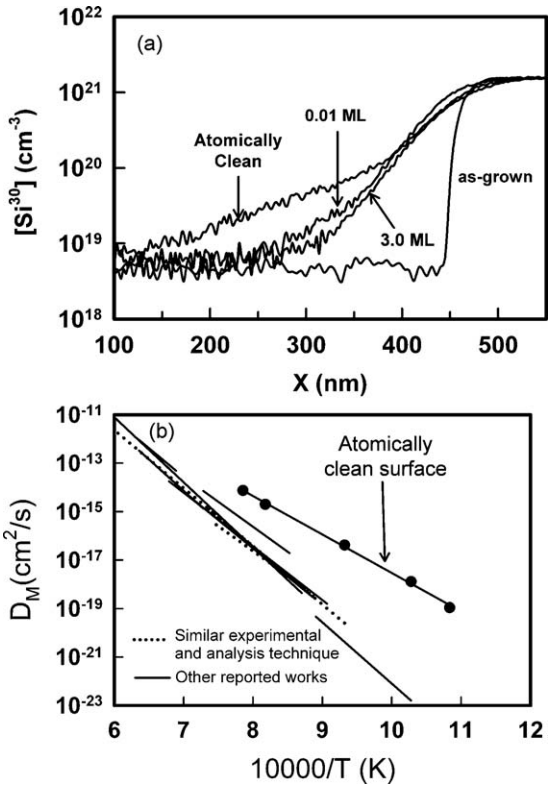

Fig. 9. (a) Profiles of ^{30}Si in isotopic heterostructures. Depth is measured with respect to the surface. Specimens (other than as-grown) supported various coverages of N, and were heated at 1100 °C for 60 min. (b) Self-diffusion coefficients in *n*-doped Si for the atomically clean (100) surface compared with literature reports with various methods and doping levels. After [48].

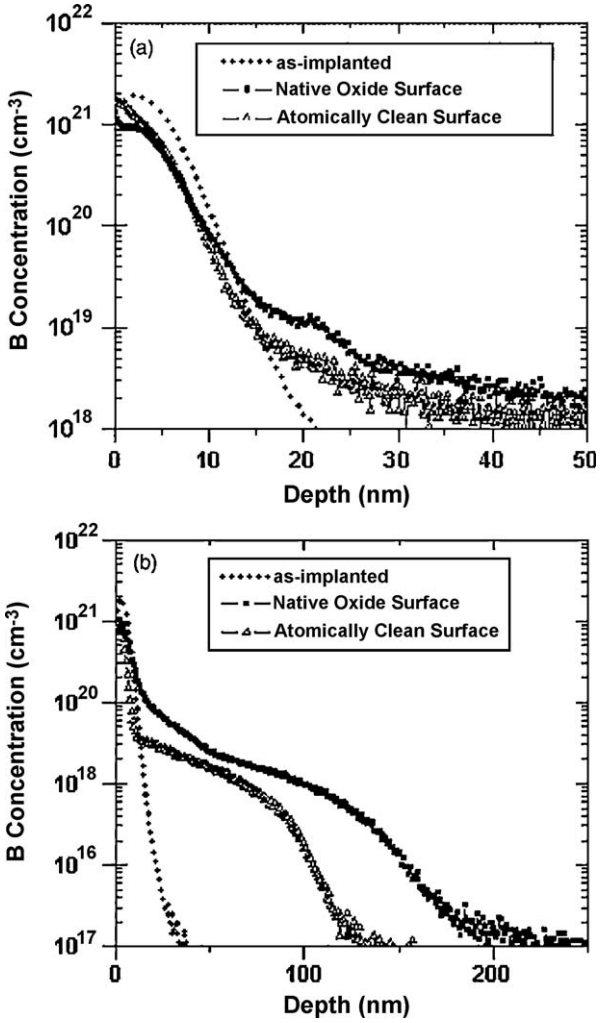

Fig. 10. Secondary ion mass spectroscopy (SIMS) profiles of 500 eV B implant in silicon with prior 15 keV Ge preamorphizing implant. Annealing was performed at (a) 700 °C and (b) 800 °C for 60 min. The atomically clean surface leads to reduced diffusion in both cases. After [156].

activation, as well as a substantial reduction of end-of-range defects due to annihilation of excess interstitials emitted from those defects.

A second mechanism exists for a surface or interface to control bulk defects: through electrostatics [47,158,159]. Atomically clean semiconductor surfaces often support electrically charged defects that become electrically charged by withdrawing or injecting electrons into the underlying bulk. The exchange of charge takes place between the surface and layer of the underlying bulk – the "space charge region." The charge exchange, together with the variation of electric potential within the space charge region, creates an electric field as shown in Fig. 11 in the case of *p*-type bulk doping. When the background carrier concentration is large, the space charge region becomes very narrow and leads to large gradients in electric potential and therefore a high local electric field. This field can attract or repel charged bulk defects from the surface, depending upon their charge state. The change in electric potential can also induce dopant pileup within the first 4–10 nm of the surface [159]. If the diffusing point defects are capable of assuming multiple charge states and the change in near-surface electric potential is large enough, the defects near the surface change their charge state from the values they would have in the deep bulk. In this way, near-surface defects that would otherwise be repelled from the surface might experience a neutral interaction or even an attraction, leading to pileup.

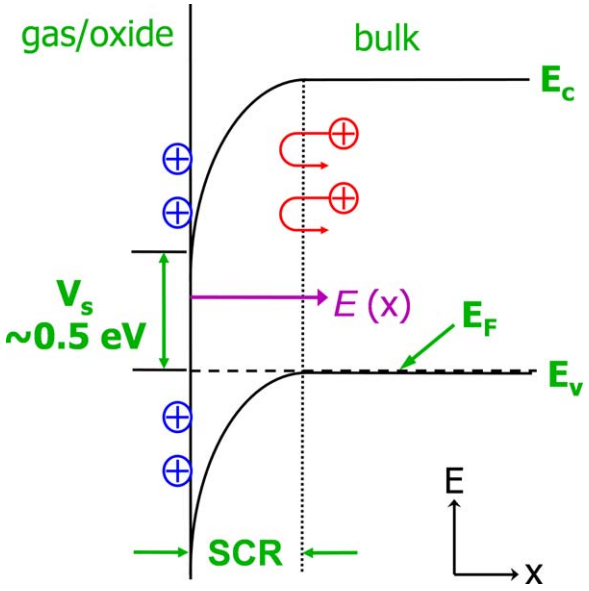

Fig. 11. Schematic diagram showing how electric fields that build up at surfaces or interfaces due to band bending can interact with charged defects. In typical cases, the defects are repelled from the surface.

3.7. Photostimulation effects

The need for precise defect control when fabricating devices of nanoscale dimensions, coupled with the optical methods commonly employed for making *pn* junctions, raises the question of whether illumination acts merely to create heat or also to affect other aspects of defect behavior. Indeed, optical photostimulation excites the formation of extra charge carriers. The additional carriers in turn can alter the average charge state of defects that are present. Since charge state affects both the formation energy and diffusion constants of point defects [44,45], effects can propagate through into phenomena such as defect diffusion.

This chain of events was first postulated in the early 1990s [160], but has been unambiguously demonstrated for bulk diffusion only recently through experimental techniques that decouple heating and illumination [161–165]. For self-diffusion in *n*-type Si, illumination increases the diffusivity by a factor of up to 25 in response to optical fluxes near 1.5 W/cm^2 (Fig. 12). Fig. 13 shows the dependence of photostimulated diffusivity versus intensity. The degree of illumination enhancement varies with both temperature and intensity. Importantly, no photostimulation

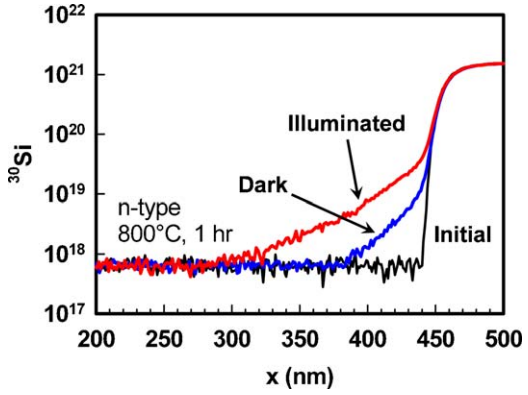

Fig. 12. Secondary ion mass spectroscopy (SIMS) profile of ^{30}Si in isotopic heterostructures showing illumination enhancement at 800 °C for 1 h (*n*-type). After [165].

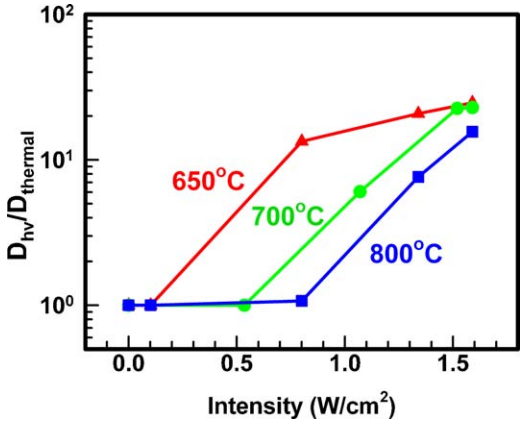

Fig. 13. Illumination enhancement factor versus illumination intensity for *n*-type Si.

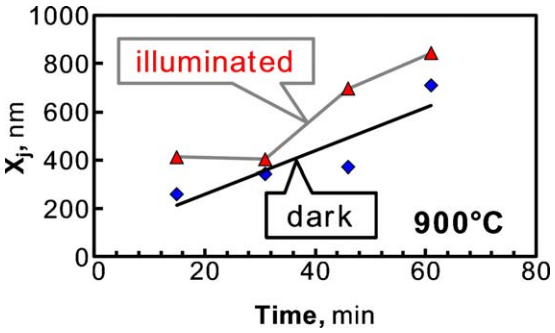

Fig. 14. Junction depth X_j for B implanted into Si (500 eV, 1×10^{15} atom/cm^2) through thermally grown oxide and annealed. Photostimulation intensity of 2 W/cm^2 stimulates more diffusion, leading to a deeper junction. However, details of the results change if the oxide is grown natively rather than thermally.

effects are observed for *p*-type material under similar experimental conditions. The difference in behavior between *n*- and *p*-type material gives strong evidence that the observed enhancement in *n*-Si is genuine, and not an artifact of a spurious heating effect.

The exponential profile shapes in Fig. 12 represent the signature of mass transport via a fast-moving intermediate species. That species turns out to be the Si interstitial under the conditions of these experiments [166]. Through the use of Shockley-Read statistics [167] as extended by Simmons and Taylor [168], a non-equilibrium steady-state model can be formulated [136] to describe the charge state of the interstitials. Such analysis shows that both the site-to-site hopping rate and the concentration of mobile interstitials are affected by illumination.

There is similar experimental evidence for photostimulated diffusion of boron and arsenic implanted into silicon [162,169], with example data for boron shown in Fig. 14 [170]. Both the diffusion and activation of these dopants vary significantly with illumination at the 1–2 W/cm^2 level. In the case of boron, some of the behavior appears to originate from mechanisms distinct from photostimulated changes in charge state of the mobile species. Instead, photostimulation changes the charge state of defects residing at a nearby surface or interface. Those defects can interact electrostatically with charged bulk defects as described in the previous section. Thus, changes in the amount of charge at the surface propagate through into changes in the ability of the surface to absorb bulk defects or to induce near-surface dopant pileup.

4. Non-Si microelectronics

Semiconductors apart from Si also find important uses in microelectronics. Some of the earliest devices were based on

germanium, and this element is enjoying a resurgence of interest. Ge possesses many beneficial electrical properties, including a higher carrier mobility compared to Si. From a processing perspective, Ge permits the use of lower temperatures for dopant activation and defect reduction [171] (although ion implantation produces comparatively more damage [172]). Until recently, the main drawback to Ge compared to Si has been the absence of a stable native oxide for Ge. However, mainstream Si technology is shifting away from its reliance on the native oxide, and is moving toward other high-dielectric constant materials such as hafnium-based oxides. The absence of a good native oxide is therefore no longer so problematic for Ge.

Due to the many similarities of Ge and Si, the defect engineering techniques already developed for Si can be employed readily for Ge. Examples include the use in Ge of flash annealing [173], laser annealing [174,175], plasma doping [174], and vacancy engineering [176]. Specific details do differ from the Si case, however. For example, boron diffuses rather slowly in Ge, and has low solid solubility [172,177–179]. Yet common *n*-type dopants such as P, As and Sb diffuse rapidly even at relatively low temperatures near 500 °C [180,181]. Hence, diffusion and activation problems tend to be worse for *n*-type dopants in Ge than for *p*-type – opposite to the case of Si.

Compound semiconductors such as III–V and II–VI materials comprise another class of constituents for microelectronics. By mixing different cationic and anionic elements (*e.g.*, Ga and In in $Ga_xIn_{1-x}As$), the band gap of the alloy material can be tuned. This property enables the fabrication of heterojunctions and high electron mobility transistors (HEMTs). Compound semiconductors find widespread use in optoelectronic devices such as light emitting diodes and laser diodes, as well as PV cells. In fact, PV cells with the highest efficiencies have been fabricated using multiple layers of compound semiconductors [182,183].

The main challenge of fabricating such devices originates from the need for multiple layers of different composition with few defects. The varying composition of the layers to achieve the required band gaps alters the lattice constants, which complicates the creation of perfect epitaxial layers. Lattice mismatch between layers fosters the formation of threading dislocations that degrade device performance. Two primary methods have been employed to overcome these problems: step grade growth and epitaxial lateral overgrowth. Step grade growth [182,184] exploits the fact that the lattice constant of compound semiconductors is proportional to the ratio of the constituting elements. By growing multiple layers with a gradually changing ratio of the components, it is possible to vary the lattice constant gradually through the layers. This gradation reduces the stress between layers and inhibits the formation of dislocations. In epitaxial lateral overgrowth (Fig. 15) [185,186], the base material grows on the substrate through a mask and eventually spreads laterally on top of the mask. The presence of the mask reduces the formation of dislocations, and any stress that was formed by the mask is reduced by the lateral overgrowth. The concentration of threading dislocations decreases significantly.

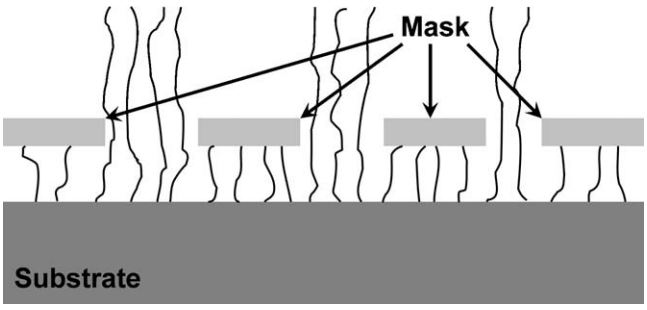

Fig. 15. Schematic of epitaxial lateral overgrowth. Black lines depict dislocations.

In addition to these extended defects, other defects that form deep states within the band gap and trap charge also degrade the performance of devices. For example, gate-lag effects, current collapse, and gate leakage currents in HEMTs have been associated with the surface states of the material [187–191]. More recently, these phenomena have been attributed to surface charge states, surface defects and also nitrogen vacancies (for nitride semiconductors) [188,192,193]. By the use of surface treatment or surface passiviation, *e.g.*, H_2, N_2, or NH_3 plasma treatment, the leakage current has been found to decrease significantly [187,188,191].

Field-effect transistors (FETs) are three-terminal devices that use a voltage applied to a controlling gate terminal to control the conductivity of a nearby channel connecting the source terminal to the drain terminal. Recently, nanowires (NWs) have found use as the channels in FETs. Several materials have been employed, including Si, GaAs, ZnO, SnO_2, and others. The performance of these devices depends upon the doping state, NW size, and presence of surface states and bulk defect states. As mentioned previously, various surface treatments alter the electronic properties of the NWs. Bulk-oriented defect engineering methods may damage the NWs, and the large surface-to-volume ratio points to surface-based methods as the most effective route for defect engineering. For example, Keem et al. [194] observed an increase in the transconductance (the ratio of the current change at the output port to the voltage change at the input port) and mobility in ZnO NW FETs after the devices were annealed in a H_2/Ar environment. This step reduced the trap charges and contaminants on the surfaces of the NWs. Chang and coworkers [195] found that passivating the surfaces of ZnO NWs with a SiO_2/Si_3N_4 bilayer increases the device performance (Fig. 16) in terms of subthreshold swing (which quantifies how sharply the transistor is turned off by the gate voltage), on/off current ratio, and carrier mobility. Lao and coworkers [196] used various types of carboxylic acid self-assembled monolayers with different terminal groups (*e.g.*, stearic acid, lysine, dodecanedioic acid, mercapto-acetic acid, and perfluorotetradecanoic acid) to treat ZnO nanobelts – ribbon-like nanostructures with a rectangular cross section. After treatment, the nanobelts exhibited an increase in conductance by a factor of 10^6, a change from a Schottky contact to an ohmic contact, and greatly improved photoconductivity and gas sensing response. Fig. 17 shows a schematic of the mechanism.

5. Metal oxides

The science base for accomplishing defect engineering in metal oxide semiconductors is less well developed than for the semiconductors used for electronic devices. Metal oxides always contain at least two primary elements (as distinct from the elemental semiconductors Si and Ge), and the oxides often lose oxygen to the gas phase upon heating. Defect chemistry is therefore more complicated. Electrical characterization of the defects (a primary tool in electronic devices) is more difficult to accomplish in metal oxides, especially those with large band gaps. Determination of carrier type and concentration is problematic because the contacts employed for four-point-probe or Hall-effect measurements need to obey Ohm's Law but actually behave as diodes. Alternative approaches by capacitance-voltage measurements should work in principle for thin film configurations. For a typical oxide such as TiO_2, however, the resulting values of carrier concentration vary widely, and the data are often misinterpreted [197–200]. For polycrystalline material, electrically active states at grain boundaries can contribute to the carrier concentration at magnitudes that dominate the bulk crystallites (in some cases).

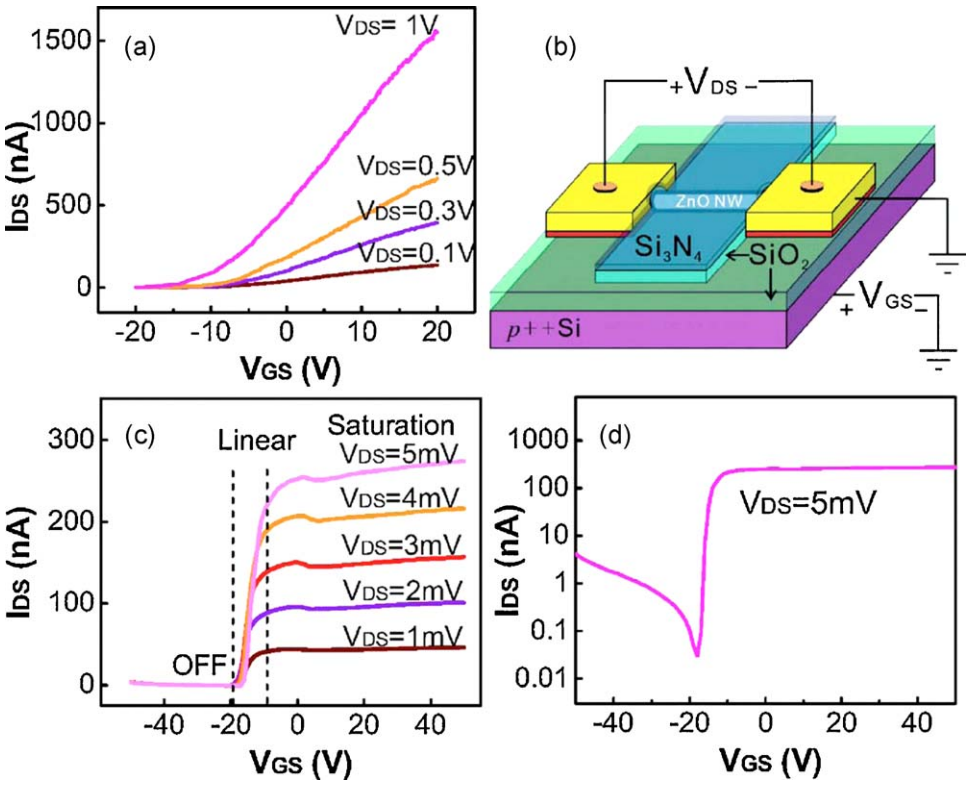

Fig. 16. Transport measurements present (a) I_{DS}–V_{GS} curves of a ZnO nanowire FET without surface treatments showing typical *n*-type semiconducting behavior. (b) Schematic of surface passivated ZnO nanowire FET with SiO_2/Si_3N_4 bilayer covering the nanowire channel. (c) I_{DS}–V_{GS} of a surface treated nanowire FET exhibits significantly enhanced on/off ratio and transconductance. (d) Semilog plot demonstrates a tenfold reduction in the subthreshold swing. At large negative gate voltages, band bending gives rise to hole conduction. Reprinted with permission from [195], copyright 2006 American Institute of Physics.

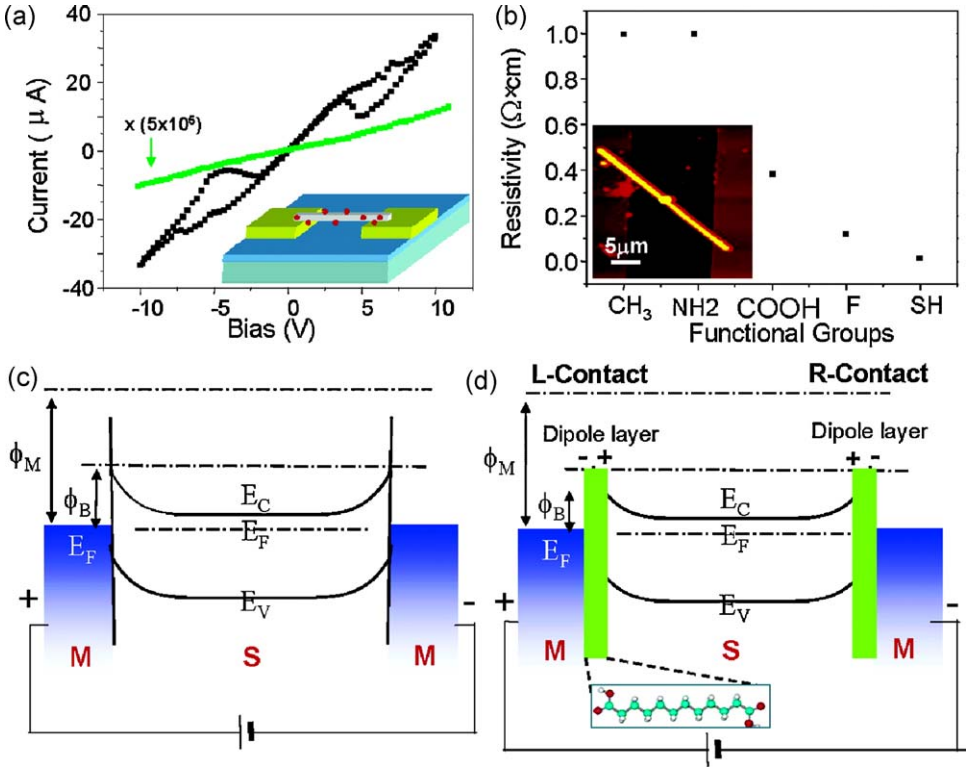

Fig. 17. (a) *I–V* characteristics of a ZnO nanobelt (NB) functionalized with the self-assembled thin molecule layer, $HOOC(CH_2)_{10}COOH$ (black line), and an untreated ZnO NB sample. The current of the untreated NB is magnified by 5×10^5 times for comparison purpose. Note: no Pt was deposited at the contacts so that the measured current for the untreated NB is low. Inset is a schematic view of the nanobelt device. (b) Resistivity of the NBs coated with different molecules. The lower inset image is an AFM image of a coated NB lying across two electrodes. (c) Energy-level diagram of metal/semiconductor/metal interfaces; ϕ_M is the work function of the metal. There is an energy barrier ϕ_B between the metal contact and the untreated NB. (d) Energy-level diagram of the Au electrode and a ZnO NB with a thin molecular layer between. The molecules form an interface dipole layer, which helps to decrease the energy barrier between the NB and Au. Reprinted with permission from [196], copyright 2007 American Chemical Society.

Additionally, the bulk and/or grain boundary states whose energies lie deep within the band gap contribute to the carrier concentration in a way that depends upon applied voltage [201]. Despite these problems, attempts to engineer the defects in metal oxides continue to grow, especially in applications involving gas sensors and photocatalysis.

5.1. Gas sensors

Gas sensors often employ nanoscale structures composed of semiconducting metal oxides to detect gases such as CO, NO_x, O_2, and others [202–205]. The gases stimulate a change in electrical properties of the sensor material upon adsorption. As gas molecules adsorb, electrons may be drawn to the surface or injected into the bulk, leading to a change in the width of the near-surface space charge region. When the semiconductor is a thin wire or film, this change induces a change in the overall resistivity, which can be detected in turn via current flowing wire or film. Defects play an important role in two respects. Surface vacancies frequently serve as the adsorption sites for gas molecules. Bulk defects (either native or substitutional dopants) are often charged and thereby determine the behavior of the space charge region in response to charge injection or withdrawal at the surface. Early gas sensors were fabricated in the form of films, but the trend in recent years has been toward smaller crystallite size and larger surface areas (Fig. 18) [206,207]. Indeed, nanocrystals, nanowires and nanobelts have found increasing use in gas sensors because of high surface-to-volume ratios. Moreover, nanowires are gaining additional interest as NW FETs became available [202,204,206,208]. These NW FETs exhibit enhanced sensitivity, as their electronic response can be optimized through control of the applied gate voltage. In addition, the application of an appropriate gate potential can also prompt electron driven desorption of the gas molecules, effectively "resetting" the sensor to the initial state in a simple manner (Fig. 19) [208]. This feature is especially useful for operation at room temperature, where thermal desorption is impractical.

In the absence of such an FET configuration, however, optimization of electrical response must be accomplished through doping and defect control. Oxygen vacancies tend to be the dominant electrically active (*i.e.*, charged) defect in metal oxides. Oxygen vacancy control has been achieved by controlling gas-phase oxygen concentration during deposition or by post-treatment in either oxygen or reducing atmospheres [209,210]. Foreign-atom dopants

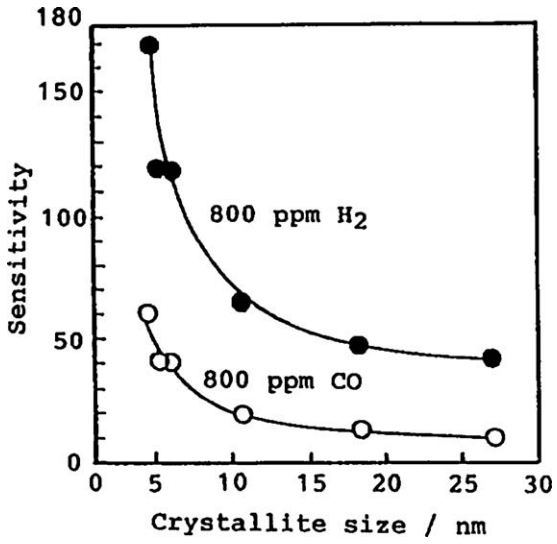

Fig. 18. Influence of SnO_2 crystallite size on gas sensitivity to 800 ppm H_2 and 800 ppm CO in air at 300 °C (elements sintered at 400 °C). Reproduced from [207].

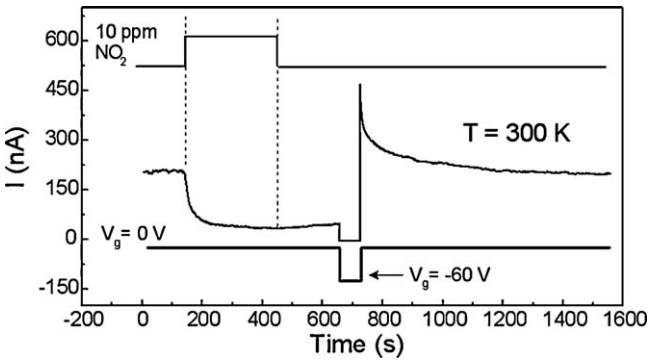

Fig. 19. ZnO nanowire FET sensing response to 10 ppm NO_2 and the conductance recovery process caused by a −60 V gate voltage pulse. Reprinted with permission from [208], copyright 2005 American Institute of Physics.

are typically introduced concurrently during growth of the sensor material [211,212]. This approach obviates the need for a separate doping step and yields spatially uniform doping. However, the method provides little direct control over native defects, which are often present in large concentrations. As an alternative to *in situ* doping, ion implantation has also been used as a post-deposition doping method [213–215]. In addition to introducing dopants, this method also induces point defects on the surface, which increases the concentration of reactive sites, thus enhancing the sensitivity of the sensor. One problem is that ion implantation creates many additional native defects. Also, the ion beam is directional, and it can be difficult to obtain uniform doping for configurations such as nanowires, where the structure is non-planar. A possible way to overcome this difficulty is by employing plasma based doping techniques. With this method, dopants may be implanted perpendicular to the surface regardless of orientation and can ensure uniform doping of non-planar structures.

While the conductance method has been used extensively for gas sensing applications, it also suffers many difficulties in creating good contacts due to the possible formation of Schottky barriers between the sensor material and the metal contacts, as well as difficulties in fabricating accurate contacts due to the small size of the wires. In an attempt to overcome these difficulties, a completely different method of detection based upon photoluminescence (PL) has been developed. Several metal oxides with wide band gaps (equivalent to ultraviolet band-to-band optical absorption) exhibit PL emission in the visible-light range. The defects responsible for this emission remain unclear. Most literature reports agree that oxygen vacancies play an important role, whether directly or indirectly [216]. PL intensity tends to rise as feature sizes shrink, suggesting that surface defects may also play a role [202,217]. For example, Faglia et al. [218] have observed that NO_2 adsorption quenches the visible PL emission in SnO_2 nanobelts. Furthermore, very low concentrations (in the ppm range) yield noticeable effects, pointing to the possibility of applications in gas sensing (Fig. 20). Similar effects have been found for NO_2 on ZnO nanowires [217,219]. In this latter case, selectivity with respect to other important gases is good; the response was unaffected by the presence of CO and perturbed only slightly by gas-phase water or ethanol. Fig. 21 shows that the response changes by less than 5% difference for either 70% relative humidity or 1000 ppm of ethanol [217].

The mechanism of gas detection with PL resembles the conductance method in some respects. Gas molecules adsorb on the surface, which induces a change in a particular defect type within the material, which in turn alters the PL. It is thought that NO_2 adsorption creates non-radiative recombination paths for electrons and holes, which reduces PL emission [202,216]. This

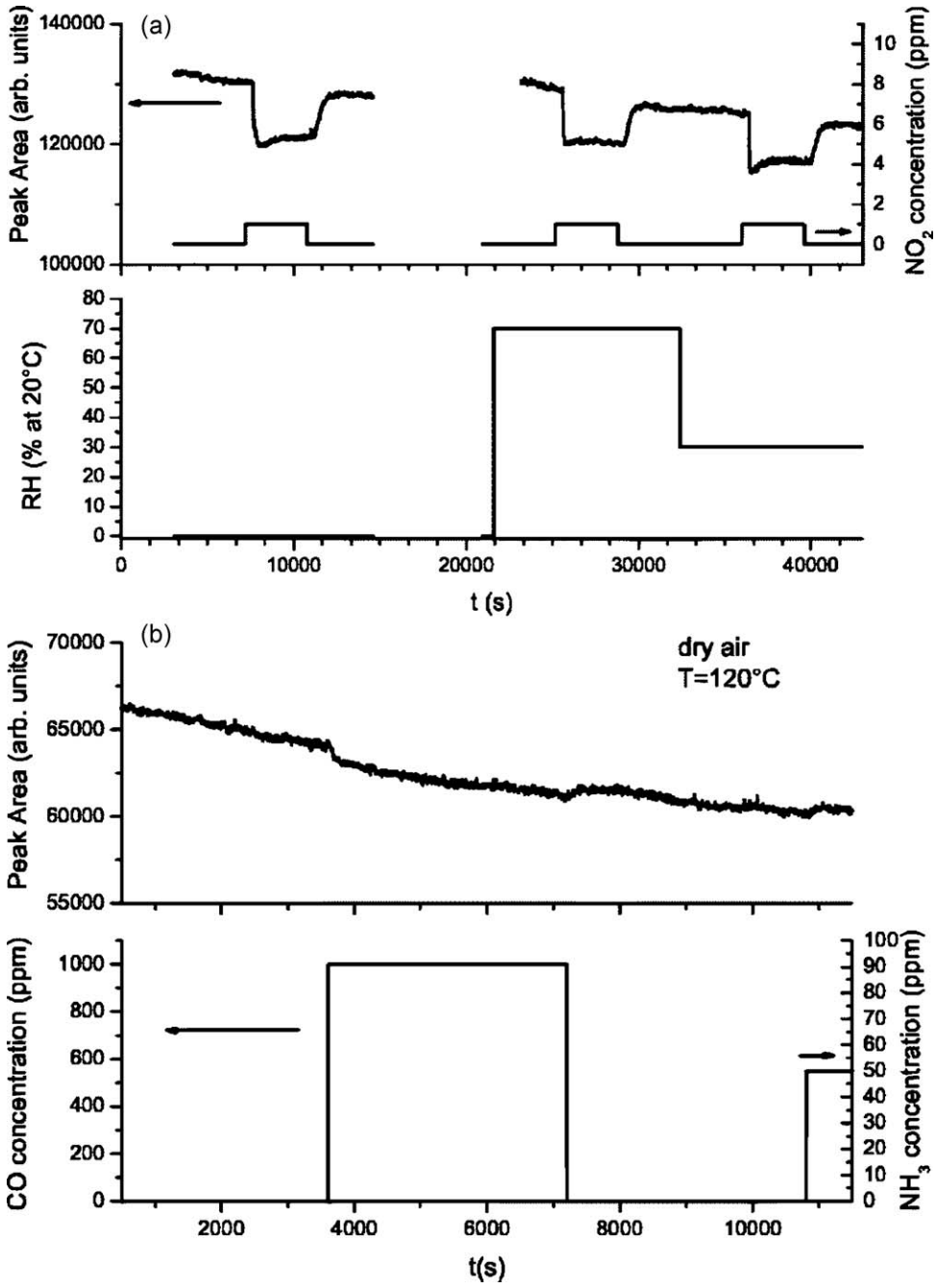

Fig. 20. Kinetic response (peak area intensity) of SnO_2 nanobelts toward (a) 1 ppm of NO_2 at 120 °C in dry air, in relative humidity (RH) = 70% and at 20 °C in RH = 30% and (b) 1000 ppm of CO and 50 ppm of NH_3 at 120 °C in dry air. Dynamic is fast, reversible, and unaffected by humidity changes. Reprinted with permission from [218], copyright 2005 American Institute of Physics.

mechanism permits the construction of relatively simple devices. Since the quenching does not lead to spectral shifts in the PL peak, a combination of an LED for excitation and a photodiode for detection suffices for sensing. Combination of conductive and PL mechanisms within the same device could lead to improved sensitivity and especially gas selectivity.

Although semiconductor-based gas sensors hold much promise, the science base clearly needs further development before solidly based defect engineering can transpire.

5.2. Photocatalysis

In photocatalysis, illumination creates charge carriers within the semiconductor that migrate to the surface where they drive chemical reactions. Although the form of the material can be thin films (as in self-cleaning windows) or pellets, the constituents of the macroscopic catalyst are typically small crystalline particles a few tens of nanometers in diameter that are pressed or sintered together. Photocatalysis applications include air pollutant mitigation, degeneration of biological wastes, water purification, and direct splitting of water into hydrogen and oxygen for fuel. Many oxide semiconductors exhibit photocatalytic behavior, such as TiO_2 [220–222], ZnO [223,224], SnO_2 [225,226] and In_2O_3 [227,228]. Some of these materials have been commercialized for photocatalysis [220–222]. TiO_2 has shown the greatest potential due to its low cost and high stability against degradation by chemical attack or prolonged illumination [41,229].

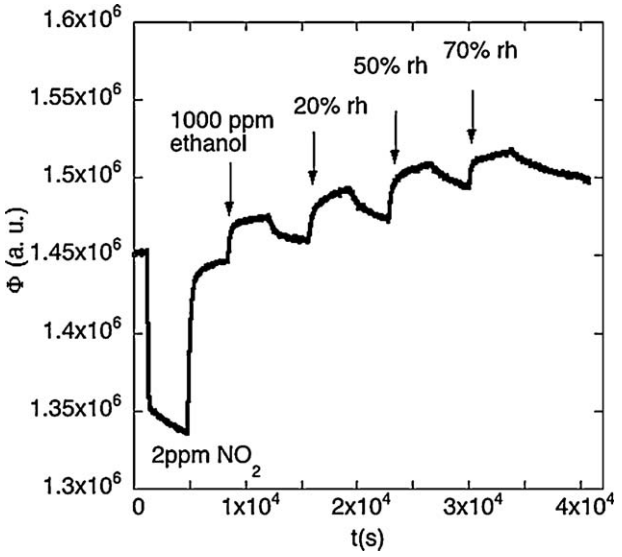

Fig. 21. Dynamic photoluminescence quenching of ZnO nanowires versus time as NO_2, ethanol and relative humidity (RH) are introduced into the test chamber. The sensor was kept at room temperature. The relative response to ethanol concentration (1000 ppm) is 1.5% while the PL increase with RH gives relative response of 2.8%, 3.9% and 4.6% respectively to 20%, 50% and 70% RH. Reproduced from [217].

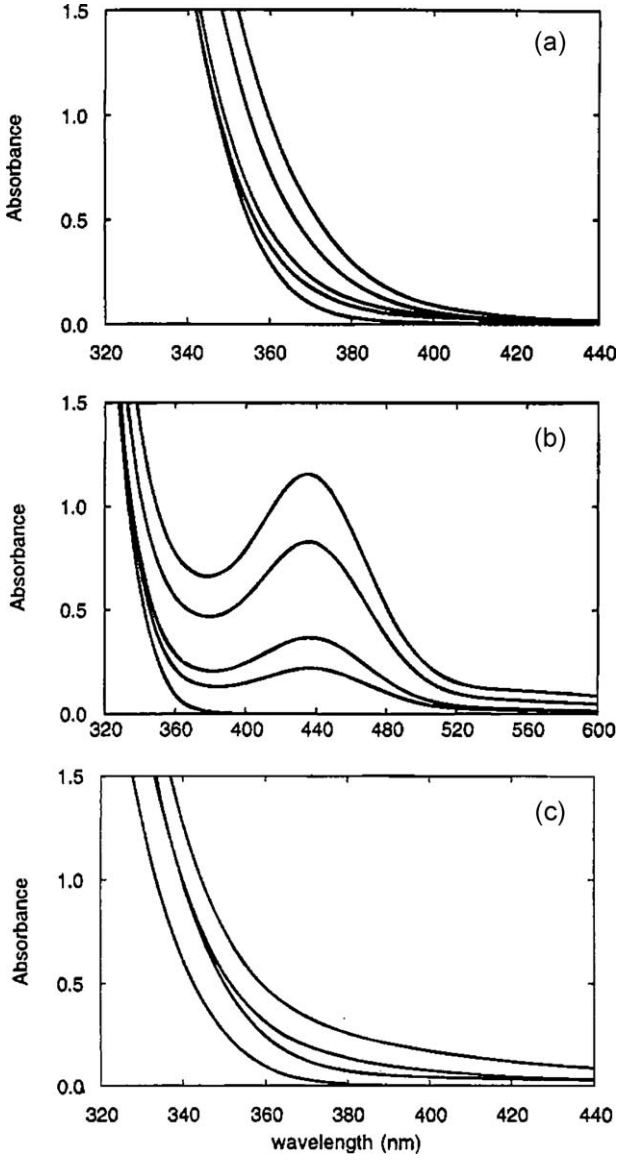

Fig. 22. Absorption spectra of (a) Fe^{3+} doped quantum (Q)-sized TiO_2 (1.34 g/L) at 0.0, 1.0, 2.0, 5.0, and 10.0% Fe^{3+} concentrations (from left to right), (b) Ru^{3+}-doped Q-sized TiO_2 (0.5 g/L) at 0.0, 0.5, 1.0, 2.0 and 3.0% Ru^{3+} concentrations (from bottom to up), and (c) undoped, Rh^{3+} (3.0%), V^{4+} (3.0%), and Mn^{3+} (3.0%) Q-sized TiO_2 at 0.5 g/L (from left to right). Reprinted with permission from [230], copyright 1994 American Chemical Society.

Most photocatalysis applications seek to employ photons originating from the sun. The most attractive metal oxides, however, have large band gaps (*e.g.*, 3.2 eV for anatase TiO_2) that confine photoabsorption to the ultraviolet or blue end of the visible spectrum. The vast majority of solar irradiation lies at longer wavelengths. To increase per-photon efficiency of photocatalysis, the band gaps need to be reduced. Many methods have been tried.

One method employs transition metal doping. Elements such as Fe, V, Cr, and Co have been introduced into TiO_2 to extend the light absorbance to the visible region (Fig. 22) [230,231]. However, results for photocatalytic activity have been mixed. High levels of metal doping do indeed reduce the band gap, but they also create non-radiative recombination centers that destroy photogenerated carriers and reduce the overall photocatalytic activity [231], although some co-doping strategies have been proposed to mitigate this problem [232]. Metal doping TiO_2 also reduces stability under heat treatment and promotes conversion to the rutile form [231], which is less active than anatase [233]. Metal dopants can exist as cations in the solid solution or form segregated clusters of metal oxides within the photocatalyst. The mechanisms by which such structures influence the photocatalytic activity are complex and vary depending upon the material. Thus, the photoreactivity of doped TiO_2 appears to be a complex function of the dopant concentration, the energy levels of dopants within the TiO_2 lattice, their electronic configuration, the spatial distribution of dopants, and the light intensity [230]. Part of the complexity arises from the fact that native defect concentrations (and their associated charge states) are rarely monitored in typical photocatalysis studies, let alone controlled [41].

Non-metal anion doping has also been investigated in depth. For example, nitrogen doped TiO_2 is capable of visible-light photodegradation of methylene blue and gaseous acetaldehyde (Fig. 23) [234]. Nitrogen atoms substitute into lattice oxygen sites and narrow the band gap by mixing N2p and O2p states. Introduction of nitrogen has been accomplished by methods ranging from amination and nitration to ion implantation and sputtering [229,234–238]. In most cases, the photocatalytic activity increases, but as with metal dopants, there exists evidence that nitrogen incorporation also creates recombination centers [238]. Carbon has also been examined as an anionic dopant in TiO_2 due to a significant overlap between the O2p state and the carbon states near the valence band edge [239], even though C can substitute on both Ti and O sites [240]. Such doping has reduced the band gap energy to 2.32 eV, and a photoconversion efficiency of up to 8% (Fig. 24) [241]. Park et al. [242] synthesized nanotube arrays of carbon doped TiO_2 with photocurrent and water splitting efficiency under visible-light illumination (>420 nm) far exceeding that of corresponding undoped TiO_2 arrays. Other non-metals such as S, Br, and Cl have also been used as dopants to decrease the TiO_2 band gap and thereby increase photoactive reactivity [243–245]. Anionic doping has been carried out in other metal oxides as well to reduce the band gap. Nitrogen has been doped into ZnO for photocatalytic degradation applications [246], while C and N have found use in water splitting by In_2O_3 [227,228].

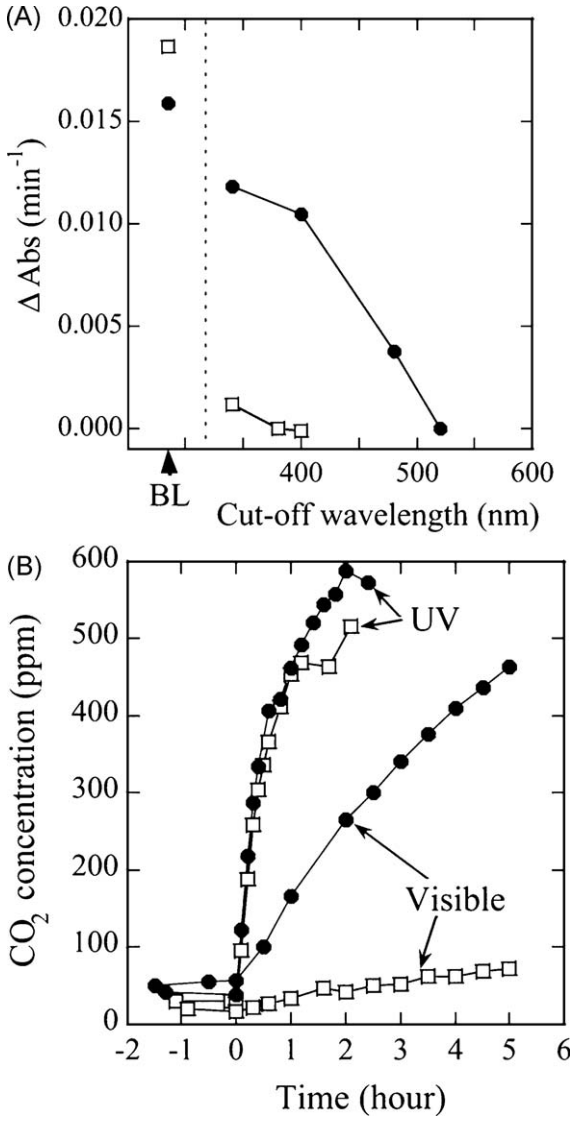

Fig. 23. Photocatalytic properties of $TiO_{2-x}N_x$ samples (solid circles) compared with TiO_2 samples (open squares). (A) Decomposition rates [measuring the change in absorption of the reference light (Δ_{abs})] of methylene blue as a function of the cutoff wavelength of the optical high-path filters under fluorescent light with the integrated photon flux of 2.45×10^{-9} einstein (E) s^{-1} cm^{-2} between 350 and 520 nm, compared with the results under black light (BL) illumination with the integrated photon flux of 3.51×10^{-9} E s^{-1} cm^{-2} in the UV range. (B) CO_2 evolution as a function of irradiation time (light on at zero) during the photodegradation of acetaldehyde gas [with an initial concentration of 485 parts per million (ppm)] under UV irradiation (BL with a peak at 351 nm and the light power of 5.4 mW cm^{-2}) and visible irradiation [fluorescent light cut by the optical high-path filter (SC42, Fuji Photo Film), with a peak intensity at 436 nm and a light power of 0.9 mW cm^{-2}]. Reprinted with permission from [234], copyright 2001 American Association for the Advancement of Science.

Some defect engineering for photocatalysis has avoided doping entirely and attempted simply to control the intrinsic defect concentration. For example, strong chemical reduction of TiO_2 promotes optical absorbance in the visible region [247–250], and Ti^{3+}-V_O-Ti^{3+} centers may serve as catalytically active centers in photoassisted oxidation of water (where V_O represents the oxygen vacancy) [251]. However, high-temperature heating in reducing atmospheres leads to the formation of the rutile phase, which is not favorable for photocatalytic reactions [233]. Thus, low temperature methods must be employed. Ihara and coworkers [249,250,252] used a radio-frequency H_2 plasma to reduce TiO_2 at lower temperatures and found an increase in the photocatalytic activity of benzoic acid, propanol, and NO_x oxidation. The effect on

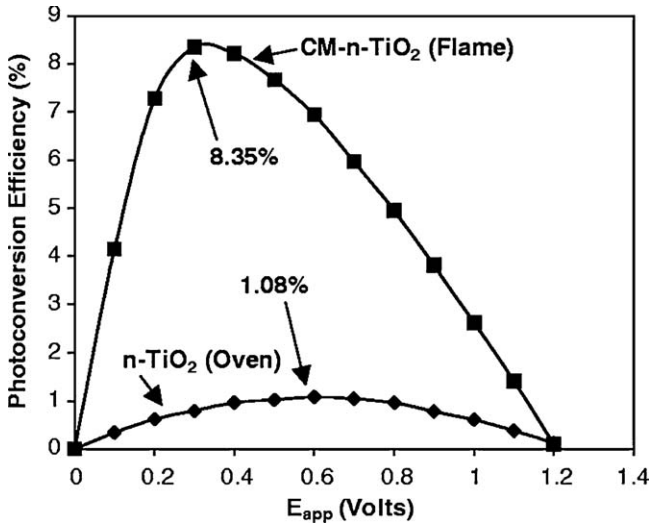

Fig. 24. Photoconversion efficiency as a function of applied potential E_{app} at chemically modified n-TiO_2 (flame-made) and the reference n-TiO_2 (electric tube furnace or oven-made) photoelectrodes under xenon lamp illumination at an intensity of 40 mW cm^{-2}. Reprinted with permission from [241], copyright 2001 American Association for the Advancement of Science.

NO_x oxidation is shown in Fig. 25. Oxygen vacancies also appear to promote photocatalysis by ZnO [253].

6. Prospects for defect engineering

Considerable progress has been made over the past decade or so in controlling the behavior of defects in semiconductors, driven in large measure by the need to manipulate material properties at the nanoscale. Some methods have become mainstream commercial techniques, especially in electronic devices. Yet many challenges remain, as unambiguous experiments are difficult and computational tools are often unreliable. Furthermore, it is difficult to predict the charged defect behavior of a given semiconductor by comparing it to a similar material [44,45]. For example, vacancies and self-interstitials in silicon and germanium do not display the same set of stable charge states.

Regarding experimental methods, certain defect properties can sometimes be derived from direct methods such as electron paramagnetic resonance, positron annihilation spectroscopy, and deep level transient spectroscopy [44,45]. Yet not all these techniques are well suited to every semiconductor. Experiments are often hampered because most point and extended defects exist at low concentrations and are therefore difficult to observe. As a result, easier-to-implement indirect methods have found common use for inferring information about the type and concentration of bulk point defects. For example, self-diffusion measurements can be made with an isotopic tracer together with secondary ion mass spectroscopy [48,254,255]. Yet such experimental results have often proven conflicting. For example, experimental results have been used to justify diffusion coefficients for the Si self-interstitial that vary by more than ten orders of magnitude at typical processing temperatures [256].

In consequence, *ab initio* quantum calculations have become commonly used atomic scale tools for investigating defect structure, thermodynamics, charging and diffusion. Yet most quantum calculations are valid only at 0 K, and mechanisms can change at higher temperatures. For example, diffusion in Si at processing temperatures appears to be governed by collective atomic motions that do not operate at lower temperatures [256]. Moreover, quantum calculations typically ignore entropic effects, some of which can change pre-exponential factors by many orders

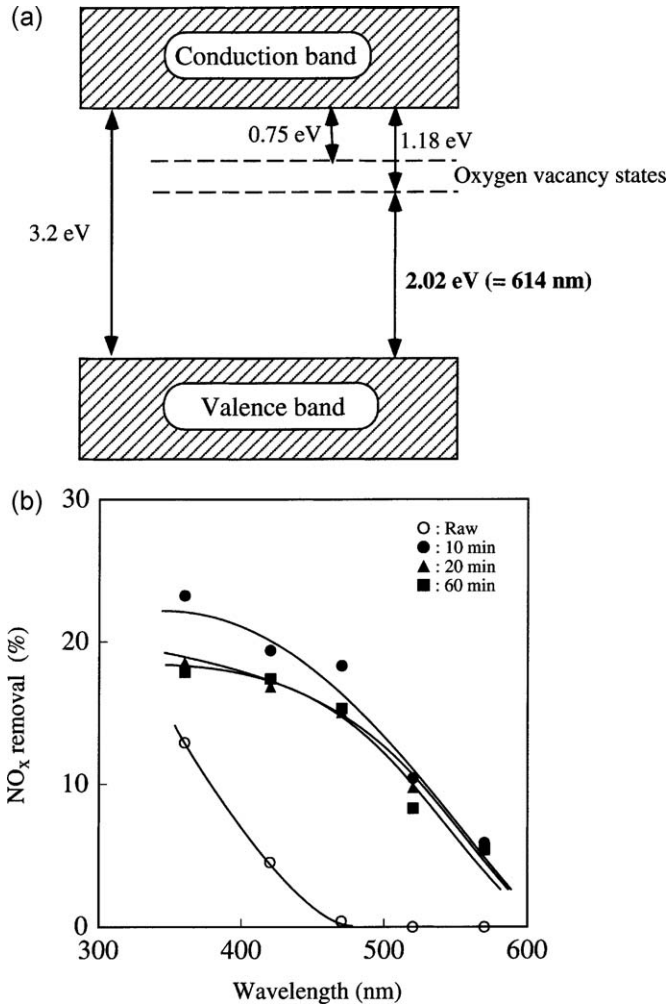

Fig. 25. (a) A proposed band structure model for anatase TiO_2 with oxygen vacancies. (b) NO_x removal percentage as a function of irradiation wavelength over the raw TiO_2 and the plasma-treated TiO_2 photocatalysts. Reproduced from [250].

of magnitude [256]. Correction schemes to improve these errors have been proposed by numerous authors, many of which have been reviewed and assessed [257]. Unfortunately, for charged and neutral defects, electrostatic errors arising from multiple interactions affect the accuracy of the formation energy [258,259]. Various correction schemes have appeared in the computational literature, but they still introduce large errors in the calculated total energies [260,261].

In light of these problems and the complexity of defect reaction and diffusion in many semiconductors, other rationally defensible procedures for estimating ionization levels, formation energies and diffusion coefficients must be accepted in place of certain truth about their values. One approach that deals directly with this problem is the statistical technique of maximum likelihood parameter estimation [262]. This method uses Bayesian statistics to estimate the most likely value for each parameter based on the available literature, and also estimates the corresponding uncertainty. The maximum likelihood approach has proven useful in predicting ionization levels for interstitial atoms in Si [5], as well as their diffusion coefficients [263] and rate constants for their exchange with the lattice [263] and the surface [48,264]. The approach can be extended by a combination of parameter sensitivity analysis [265] and the method of maximum *a posteriori* estimation [266] to yield further refinements of these quantities for use in predictive models [117].

7. Summary

Defect engineering in semiconductors has become much more sophisticated in recent years, driven by the need to control material properties at small length scales. Some methods for defect manipulation have proven quite successful, although efforts in metal oxide semiconductors lag those for the materials used in electronic devices. Promising new mechanisms have been discovered for controlling defects through low-energy ions, surface chemistry, and photostimulation. Yet for many materials no consensus exists about important properties such as which defect charge states are stable, or the values of the Fermi energies at which charge state transitions occur. Experimental determination of this information is often difficult, as defects exist in low concentrations in solids. Quantum methods are improving but remain unreliable for predicting charged defect behavior. Systems-based methods for parameter estimation may help fill the gap for the complex diffusion and reaction networks that characterize defect behavior in most key applications.

Acknowledgements

The authors gratefully acknowledge the support of the US National Science Foundation (DMR-07-04354).

References

[1] H. Bracht, MRS Bull. 25 (2000) 22–27.
[2] N. Dasgupta, A. Dasgupta, Semiconductor Devices: Modeling and Technology, Prentice-Hall, New Delhi, 2004.
[3] P.M. Fahey, P.B. Griffin, J.D. Plummer, Rev. Mod. Phys. 61 (1989) 289–384.
[4] S.M. Hu, Mater. Sci. Eng. R 13 (1994) 105–192.
[5] M.Y.L. Jung, C.T.M. Kwok, R.D. Braatz, E.G. Seebauer, J. Appl. Phys. 97 (2005) 063520.
[6] J.W. Fergus, J. Mater. Sci. 38 (2003) 4259–4270.
[7] W. Baiqi, J. Liqiang, Q. Yichun, L. Shudan, J. Baojiang, Y. Libin, X. Baifu, F. Honggang, Appl. Surf. Sci. 252 (2006) 2817–2825.
[8] Y. Zhang, A. Kolmakov, S. Chretien, H. Metiu, M. Moskovits, Nano Lett. 4 (2004) 403–407.
[9] W.W. Chow, S.W. Koch, Semiconductor-Laser Fundamentals: Physics of the Gain Materials, Springer, Berlin, 1999.
[10] S. Guha, J.M. Depuydt, M.A. Haase, J. Qiu, H. Cheng, Appl. Phys. Lett. 63 (1993) 3107–3109.
[11] G. Lutz, Semiconductor Radiation Detectors: Device Physics, Springer, Berlin, 1999.
[12] S.R. Kurtz, A.A. Allerman, E.D. Jones, J.M. Gee, J.J. Banas, B.E. Hammons, Appl. Phys. Lett. 74 (1999) 729–731.
[13] S.A. Campbell, The Science and Engineering of Microelectronic Fabrication, Oxford University Press, New York, 2001.
[14] R. Doering, Y. Nishi, Handbook of Semiconductor Manufacturing Technology, CRC Press, Boca Raton, 2008.
[15] P. Siffert, E.F. Krimmel, Silicon: Evolution and Future of a Technology, Springer, Berlin, 2004.
[16] E.C. Jones, E. Ishida, Mater. Sci. Eng. R 24 (1998) 1–80.
[17] B. Colombeau, S.H. Yeong, D.X.M. Tan, A.J. Smith, R.M. Gwilliam, C.M. Ng, K.R.C. Mok, F. Benistant, L. Chan, in: Proceedings of the 17th International Conference on Ion Implantation Technology, AIP, Monterey, CA, (2008), pp. 11–18.
[18] H.J.L. Gossmann, J. Vac. Sci. Technol. B 26 (2008) 267–272.
[19] G. Müller, Cryst. Res. Technol. 42 (2007) 1150–1161.
[20] T. Sinno, E. Dornberger, W. von Ammon, R.A. Brown, F. Dupret, Mater. Sci. Eng. R 28 (2000) 149–198.
[21] J. Vanhellemont, J. Van Steenbergen, F. Holsteyns, P. Roussel, M. Meuris, K. Młynarczyk, P. Śpiewak, W. Geens, I. Romandic, J. Mater. Sci.: Mater. Electron. 19 (2008) 24–31.
[22] E. Chason, S.T. Picraux, J.M. Poate, J.O. Borland, M.I. Current, T.D. delaRubia, D.J. Eaglesham, O.W. Holland, M.E. Law, C.W. Magee, J.W. Mayer, J. Melngailis, A.F. Tasch, J. Appl. Phys. 81 (1997) 6513–6561.
[23] A. Claverie, B. Colombeau, B. De Mauduit, C. Bonafos, X. Hebras, G. Ben Assayag, F. Cristiano, Appl. Phys. A 76 (2003) 1025–1033.
[24] L. Pelaz, L.A. Marques, M. Aboy, P. Lopez, J. Barbolla, Comput. Mater. Sci. 33 (2005) 92–105.
[25] L. Shao, J.R. Liu, Q.Y. Chen, W.K. Chu, Mater. Sci. Eng. R 42 (2003) 65–114.
[26] P.K. Chu, Plasma Phys. Control. Fusion 45 (2003) 555–570.
[27] J. Pelletier, A. Anders, IEEE Trans. Plasma Sci. 33 (2005) 1944–1959.
[28] S. Walther, R. Liebert, J. Vac. Sci. Technol. B 24 (2006) 482–488.
[29] N.E.B. Cowern, A.J. Smith, N. Bennett, B.J. Sealy, R. Gwilliam, R.P. Webb, B. Colombeau, S. Paul, W. Lerch, A. Pakfar, Mater. Sci. Forum 573–574 (2008) 295–304.

[30] R.M. Gwilliam, N.E.B. Cowern, B. Colombeau, B. Sealy, A.J. Smith, AIP Conf. Proc. 876 (2006) 181–190.
[31] A. Bratschun, J. Electron. Mater. 28 (1999) 1328–1332.
[32] J. Nakos, J. Shepard, Mater. Sci. Forum 573–574 (2008) 3–19.
[33] S. Paul, W. Lerch, Mater. Sci. Forum 573–574 (2008) 207–228.
[34] J. Foggiato, W.S. Yoo, Mater. Sci. Eng. B 124 (2005) 219–222.
[35] W. Skorupa, R.A. Yankov, M. Voelskow, W. Anwand, D. Panknin, R.A. McMahon, M. Smith, T. Gebel, L. Rebohle, R. Fendler, W. Hentsch, RTP 2005 – 13th IEEE International Conference on Advanced Thermal Processing of Semiconductors, IEEE, Santa Barbara, CA, (2005), pp. 53–71.
[36] S.O. Kucheyev, J.S. Williams, C. Jagadish, Vacuum 73 (2004) 93–104.
[37] C. Ronning, E.P. Carlson, R.F. Davis, Phys. Rep. 351 (2001) 349–385.
[38] W. Wesch, Nucl. Instrum. Methods Phys. Res. B 68 (1992) 342–354.
[39] M. Anpo, S. Dohshi, M. Kitano, Y. Hu, M. Takeuchi, M. Matsuoka, Annu. Rev. Mater. Res. 35 (2005) 1–27.
[40] M. Ni, M.K.H. Leung, D.Y.C. Leung, K. Sumathy, Renew. Sust. Energ. Rev. 11 (2007) 401–425.
[41] M.K. Nowotny, L.R. Sheppard, T. Bak, J. Nowotny, J. Phys. Chem. C 112 (2008) 5275–5300.
[42] C.G. Van de Walle, Physica B 308 (2001) 899–903.
[43] S.P. Wilks, J. Phys. D: Appl. Phys. 35 (2002) R77–R90.
[44] E.G. Seebauer, M.C. Kratzer, Mater. Sci. Eng. R 55 (2006) 57–149.
[45] E.G. Seebauer, M.C. Kratzer, Charged Semiconductor Defects: Structure, Thermodynamics and Diffusion, Springer, New York, 2008.
[46] D. Hull, D.J. Bacon, Introduction to Dislocations, Butterworth-Heinemann, Oxford, 2001.
[47] K. Dev, M.Y.L. Jung, R. Gunawan, R.D. Braatz, E.G. Seebauer, Phys. Rev. B 68 (2003) 195311.
[48] E.G. Seebauer, K. Dev, M.Y.L. Jung, R. Vaidyanathan, C.T.M. Kwok, J.W. Ager, E.E. Haller, R.D. Braatz, Phys. Rev. Lett. 97 (2006) 055503.
[49] W. Shockley, W.T. Read, Phys. Rev. 87 (1952) 835.
[50] S.M. Sze, Semiconductor Devices, Physics and Technology, Wiley, New York, 2002
[51] K. Vanheusden, W.L. Warren, C.H. Seager, D.R. Tallant, J.A. Voigt, B.E. Gnade, J. Appl. Phys. 79 (1996) 7983–7990.
[52] S.A. Centoni, B. Sadigh, G.H. Gilmer, T.J. Lenosky, T.D. de la Rubia, C.B. Musgrave, Phys. Rev. B 72 (2005) 195206.
[53] H.Y.H. Chan, K. Dev, E.G. Seebauer, Phys. Rev. B 67 (2003) 035311.
[54] C.E. Allen, R. Ditchfield, E.G. Seebauer, J. Vac. Sci. Technol. A 14 (1996) 22–29.
[55] W.C. Lee, S.G. Lee, K.J. Chang, J. Phys.: Condens. Matter 10 (1998) 995–1002.
[56] J. Tersoff, Phys. Rev. Lett. 65 (1990) 887–890.
[57] P. Mascher, S. Dannefaer, D. Kerr, Phys. Rev. B 40 (1989) 11764–11771.
[58] M.J. Puska, C. Corbel, R.M. Nieminen, Phys. Rev. B 41 (1990) 9980–9993.
[59] P.W. Tasker, A.M. Stoneham, J. Phys. C: Solid State Phys. 10 (1977) 5131–5140.
[60] R. Ditchfield, D. Llera-Rodriguez, E.G. Seebauer, Phys. Rev. Lett. 81 (1998) 1259–1262.
[61] R. Ditchfield, D. Llera-Rodriguez, E.G. Seebauer, Phys. Rev. B 61 (2000) 13710–13720.
[62] E.G. Seebauer, in: Proceedings of the 7th International Conference on Solid-State and Integrated Circuits Technology, IEEE, Beijing, 2004, pp. 1032–1037.
[63] G. Müller, Perspectives on Inorganic, Organic and Biological Crystal Growth: From Fundamentals to Applications: Based on the lectures presented at the 13th International Summer School on Crystal Growth, Park City, UT, USA, 2007, pp. 3–33.
[64] E. Dornberger, W. von Ammon, J. Virbulis, B. Hanna, T. Sinno, J. Cryst. Growth 230 (2001) 291–299.
[65] M.S. Kulkarni, Ind. Eng. Chem. Res. 44 (2005) 6246–6263.
[66] M.S. Kulkarni, J. Cryst. Growth 303 (2007) 438–448.
[67] M.S. Kulkarni, J. Cryst. Growth 310 (2008) 324–335.
[68] A. Taguchi, H. Kageshima, K. Wada, J. Appl. Phys. 97 (2005) 053514.
[69] X. Yu, D. Yang, X. Ma, J. Yang, L. Li, D. Que, J. Appl. Phys. 92 (2002) 188–194.
[70] D. Yang, J. Chen, H. Li, X. Ma, D. Tian, L. Li, D. Que, J. Cryst. Growth 292 (2006) 266–271.
[71] D. Yang, J. Chen, H. Li, X. Ma, D. Tian, L. Li, D. Que, Phys. Status Solidi A 203 (2006) 685–695.
[72] J. Vanhellemont, P. Spiewak, K. Sueoka, I. Romandic, Phys. Status Solidi C 6 (2009) 1906–1911.
[73] B. Mizuno, K. Okashita, K. Nakamoto, C.G. Jin, Y. Sasaki, K. Tsutsui, H.A. Sauddin, H. Iwai, Extended Abstracts of the 8th International Workshop on Junction Technology, IEEE, Shanghai, 2008, pp. 20–24.
[74] B. Mizuno, Y. Sasaki, C.G. Jin, K. Okashita, K. Nakamoto, T. Kitaoka, K. Tsutsui, H.A. Sauddin, H. Iwai, in: Proceedings of the 9th International Conference on Solid-State and Integrated Circuits Technology, IEEE, Beijing, 2008, pp. 1288–1291.
[75] J. Gelpey, S. McCoy, A. Kontos, L. Godet, C. Hatem, D. Camm, J. Chan, G. Papasouliotis, J. Scheuer, Extended Abstracts of the 8th International Workshop on Junction Technology, IEEE, Shanghai, 2008, pp. 82–86.
[76] A. Agarwal, H.J. Gossmann, D.C. Jacobson, D.J. Eaglesham, M. Sosnowski, J.M. Poate, I. Yamada, J. Matsuo, T.E. Haynes, Appl. Phys. Lett. 73 (1998) 2015–2017.
[77] K. Goto, J. Matsuo, T. Sugii, H. Minakata, I. Yamada, T. Hisatsugu, Technical Digest – International Electron Devices Meeting, IEEE, 1996, pp. 435–438.
[78] D. Takeuchi, N. Shimada, J. Matsuo, I. Yamada, Nucl. Instrum. Methods Phys. Res. B 121 (1997) 345–348.
[79] R. Smith, M. Shaw, R.P. Webb, M.A. Foad, J. Appl. Phys. 83 (1998) 3148–3152.
[80] S. Heo, H. Hwang, H.T. Cho, W.A. Krull, Appl. Phys. Lett. 89 (2006) 243516.
[81] Y. Kawasaki, T. Kuroi, T. Yamashita, K. Horita, T. Hayashi, M. Ishibashi, M. Togawa, Y. Ohno, M. Yoneda, T. Horsky, D. Jacobson, W. Krull, Nucl. Instrum. Methods Phys. Res. B 237 (2005) 25–29.
[82] L.A. Marques, L. Pelaz, I. Santos, V.C. Venezia, Phys. Rev. B 74 (2006) 201201.
[83] A. Renau, Extended Abstracts of the 7th International Workshop on Junction Technology, IEEE, Kyoto, 2007, pp. 107–112.
[84] C.F. Tan, L.W. Teo, C.S. Yin, J.G. Lee, J. Liu, A. See, M.S. Zhou, E. Quek, S. Chu, C. Hatem, N. Variam, E. Arevalo, A. Gupta, S. Mehta, Mater. Res. Soc. Symp. Proc. 1070 (2008) 99–104.
[85] K. Ohyu, T. Itoga, N. Natsuaki, Jpn. J. Appl. Phys. 29 (1990) 457–462.
[86] T.H. Huang, H. Kinoshita, D.L. Kwong, Appl. Phys. Lett. 65 (1994) 1829–1831.
[87] N.E.B. Cowern, B. Colombeau, J. Benson, A.J. Smith, W. Lerch, S. Paul, T. Graf, F. Cristiano, X. Hebras, D. Bolze, Appl. Phys. Lett. 86 (2005) 101905.
[88] R. Duffy, V.C. Venezia, A. Heringa, B.J. Pawlak, M.J.P. Hopstaken, G.C.J. Maas, Y. Tamminga, T. Dao, F. Roozeboom, L. Pelaz, Appl. Phys. Lett. 84 (2004) 4283–4285.
[89] D. Girginoudi, C. Tsiarapas, Nucl. Instrum. Methods Phys. Res. B 266 (2008) 3565–3576.
[90] G. Impellizzeri, J.H.R. Dos Santos, S. Mirabella, F. Priolo, E. Napolitani, A. Camera, Appl. Phys. Lett. 84 (2004) 1862–1864.
[91] J.M. Jacques, L.S. Robertson, K.S. Jones, M.E. Law, M. Rendon, J. Bennett, Appl. Phys. Lett. 82 (2003) 3469–3471.
[92] B.J. Pawlak, R. Surdeanu, B. Colombeau, A.J. Smith, N.E.B. Cowern, R. Lindsay, W. Vandervorst, B. Brijs, O. Richard, F. Cristiano, Appl. Phys. Lett. 84 (2004) 2055–2057.
[93] E. Napolitani, A. Coati, D. De Salvador, A. Carnera, S. Mirabella, S. Scalese, F. Priolo, Appl. Phys. Lett. 79 (2001) 4145–4147.
[94] V. Moroz, Y.S. Oh, D. Pramanik, H. Graoui, M.A. Foad, Appl. Phys. Lett. 87 (2005) 051908.
[95] B.J. Pawlak, T. Janssens, B. Brijs, W. Vandervorst, E.J.H. Collart, S.B. Felch, N.E.B. Cowern, Appl. Phys. Lett. 89 (2006) 062110.
[96] A. Vanderpool, M. Taylor, Nucl. Instrum. Methods Phys. Res. B 237 (2005) 142–147.
[97] K.C. Ku, C.F. Nieh, J. Gong, L.P. Huang, Y.M. Sheu, C.C. Wang, C.H. Chen, H. Chang, L.T. Wang, T.L. Lee, S.C. Chen, M.S. Liang, Appl. Phys. Lett. 89 (2006) 112104.
[98] B.J. Pawlak, R. Duffy, T. Janssens, W. Vandervorst, S.B. Felch, E.J.H. Collart, N.E.B. Cowern, Appl. Phys. Lett. 89 (2006) 062102.
[99] N. Auriac, C. Laviron, N. Cagnat, J. Singer, B. Duriez, R. Gwoziecki, G. Chabanne, C. Rando, Extended Abstracts of the 7th International Workshop on Junction Technology, IEEE, Kyoto, 2007, pp. 13–16.
[100] C.T. Liu, E.J. Lloyd, Y. Ma, M. Du, R.L. Opila, S.J. Hillenius, Technical Digest – International Electron Devices Meeting, IEEE, 1996, pp. 499–502.
[101] S.H. Yeong, B. Colombeau, K.R.C. Mok, F. Benistant, C.J. Liu, A.T.S. Wee, G. Dong, L. Chan, M.P. Srinivasan, Mater. Sci. Eng. B 154–155 (2008) 43–48.
[102] J.A. Gregus, M.F. Vernon, R.A. Gottscho, G.R. Scheller, W.S. Hobson, R.L. Opila, E. Yoon, Plasma Chem. Plasma Process. 13 (1993) 521–537.
[103] K. Tsujimoto, S. Okudaira, S. Tachi, Jpn. J. Appl. Phys. 30 (1991) 3319.
[104] J. Wong-Leung, C. Jagadish, M.J. Conway, J.D.F. Gerald, J. Appl. Phys. 89 (2001) 2556–2559.
[105] N. Nitta, M. Taniwaki, T. Suzuki, Y. Hayashi, Y. Satoh, T. Yoshiie, Mater. Trans. 43 (2002) 674–680.
[106] K. Shoji, A. Fukami, T. Nagano, T. Tokuyama, C.Y. Yang, Appl. Phys. Lett. 60 (1992) 451–453.
[107] B.A. Turkot, D.V. Forbes, I.M. Robertson, J.J. Coleman, L.E. Rehn, M.A. Kirk, P.M. Baldo, J. Appl. Phys. 78 (1995) 97–103.
[108] M.A. Nastasi, J.W. Mayer, J.K. Hirvonen, Ion-Solid Interactions: Fundamentals and Applications, Cambridge University Press, New York, 1996.
[109] B.W. Dodson, Nucl. Instrum. Methods Phys. Res. B 59–60 (1991) 481–486.
[110] A. Kuronen, J. Tarus, K. Nordlund, Nucl. Instrum. Methods Phys. Res. B 153 (1999) 209–212.
[111] S.M. Lee, C.J. Fell, D. Marton, J.W. Rabalais, J. Appl. Phys. 83 (1998) 5217–5223.
[112] D. Marton, K.J. Boyd, J.W. Rabalais, J. Vac. Sci. Technol. A 16 (1998) 1321–1326.
[113] J.W. Rabalais, A.H. Al-Bayati, K.J. Boyd, D. Marton, J. Kulik, Z. Zhang, W.K. Chu, Phys. Rev. B 53 (1996) 10781.
[114] R. Ditchfield, E.G. Seebauer, Phys. Rev. Lett. 82 (1999) 1185.
[115] R. Ditchfield, E.G. Seebauer, Phys. Rev. B 63 (2001) 125317.
[116] Z. Wang, E.G. Seebauer, Phys. Rev. B 66 (2002) 205409.
[117] Z. Wang, E.G. Seebauer, Phys. Rev. Lett. 95 (2005) 015501.
[118] Z. Wang, E.G. Seebauer, Surf. Sci. 601 (2007) 2453–2458.
[119] H.H. Lin, S.L. Cheng, L.J. Chen, C. Chen, K.N. Tu, Appl. Phys. Lett. 79 (2001) 3971–3973.
[120] E.G. Roth, O.W. Holland, V.C. Venezia, B. Nielsen, J. Electron. Mater. 26 (1997) 1349–1354.
[121] V. Raineri, R.J. Schreutelkamp, F.W. Saris, K.T.F. Janssen, R.E. Kaim, Appl. Phys. Lett. 58 (1991) 922–924.
[122] V.C. Venezia, T.E. Haynes, A. Agarwal, L. Pelaz, H.J. Gossmann, D.C. Jacobson, D.J. Eaglesham, Appl. Phys. Lett. 74 (1999) 1299–1301.
[123] S. Saito, M. Kumagai, T. Kondo, Appl. Phys. Lett. 63 (1993) 197–199.
[124] L. Shao, J.M. Zhang, J. Chen, D. Tang, P.E. Thompson, S. Patel, X.M. Wang, H. Chen, J.K. Liu, W.K. Chu, Appl. Phys. Lett. 84 (2004) 3325–3327.
[125] N.E.B. Cowern, A.J. Smith, B. Colombeau, R. Gwilliam, B.J. Sealy, E.J.H. Collart, Technical Digest – International Electron Devices Meeting, IEEE, Washington, DC, 2005, pp. 968–971.
[126] A.J. Smith, N.E.B. Cowern, R. Gwilliam, B.J. Sealy, B. Colombeau, E.J.H. Collart, S. Gennaro, D. Giubertoni, M. Bersani, M. Barozzi, Appl. Phys. Lett. 88 (2006) 082112.
[127] N.S. Bennett, N.E.B. Cowern, H. Kheyrandish, S. Paul, W. Lerch, A.J. Smith, R. Gwilliam, B.J. Sealy, in: Proceedings of the 38th European Solid-State Device Research Conference, IEEE, Edinburgh, 2008, pp. 290–293.

[128] P. Timans, J. Gelpey, S. McCoy, W. Lerch, S. Paul, Materials Research Society Symposium Proceedings, 2006, pp. 3–14.
[129] K. Adachi, K. Ohuchi, N. Aoki, H. Tsujii, T. Ito, H. Itokawa, K. Matsuo, K. Suguro, Y. Honguh, N. Tamaoki, K. Ishimaru, H. Ishiuchi, Digest of Technical Papers – Symposium on VLSI Technology, IEEE, Kyoto, 2005, pp. 142–143.
[130] Y.F. Chong, K.L. Pey, A.T.S. Wee, A. See, L. Chan, Y.F. Lu, W.D. Song, L.H. Chua, Appl. Phys. Lett. 76 (2000) 3197–3199.
[131] Y. Takamura, S.H. Jain, P.B. Griffin, J.D. Plummer, J. Appl. Phys. 92 (2002) 230.
[132] T. Ito, T. Iinuma, A. Murakoshi, H. Akutsu, K. Suguro, T. Arikado, K. Okumura, M. Yoshioka, T. Owada, Y. Imaoka, H. Murayama, T. Kusuda, Jpn. J. Appl. Phys. 41 (2002) 2394–2398.
[133] W. Skorupa, T. Gebel, R.A. Yankov, S. Paul, W. Lerch, D.F. Downey, E.A. Arevalo, J. Electrochem. Soc. 152 (2005) G436–G440.
[134] C.T.M. Kwok, R.D. Braatz, S. Paul, W. Lerch, E.G. Seebauer, J. Appl. Phys. 105 (2009) 063514.
[135] L. Wang, P. Clancy, M.O. Thompson, C.S. Murthy, J. Appl. Phys. 92 (2002) 2412.
[136] T.M. Kwok, Advanced methods for defect engineering in silicon, Ph.D. Thesis, University of Illinois at Urbana-Champaign, 2007.
[137] S. Baek, S. Heo, H. Choi, H. Hwang, J. Vac. Sci. Technol. B 23 (2005) 257–261.
[138] W. Lerch, S. Paul, J. Niess, S. McCoy, T. Selinger, J. Gelpey, F. Cristiano, F. Severac, M. Gavelle, S. Boninelli, P. Pichler, D. Bolze, Mater. Sci. Eng. B 124–125 (2005) 24–31.
[139] J. Borland, A. Mineji, W. Krull, M. Tanjyo, R. Hillard, T. Walker, Solid State Technol. 49–5 (2006) 47–54.
[140] W.S. Yoo, K. Kang, Nucl. Instrum. Methods Phys. Res. B 237 (2005) 12–17.
[141] C.H. Poon, L.S. Tan, B.J. Cho, A. See, M. Bhat, J. Electrochem. Soc. 151 (2004) G80–G83.
[142] J.A. Sharp, N.E.B. Cowern, R.P. Webb, K.J. Kirkby, D. Giubertoni, S. Gennaro, M. Bersani, M.A. Foad, F. Cristiano, P.F. Fazzini, Appl. Phys. Lett. 89 (2006) 192105.
[143] A. Florakis, D. Tsoukalas, I. Zergioti, K. Giannakopoulos, P. Dimitrakis, D.G. Papazoglou, G. Bennassayag, H. Bourdon, A. Halimaoui, Nucl. Instrum. Methods Phys. Res. B 253 (2006) 13–17.
[144] F. Torregrosa, C. Laviron, F. Milesi, M. Hernandez, H. Faïk, J. Venturini, Nucl. Instrum. Methods Phys. Res. B 237 (2005) 18–24.
[145] S. Earles, M. Law, R. Brindos, K. Jones, S. Talwar, S. Corcoran, IEEE Trans. Electron Devices 49 (2002) 1118–1123.
[146] E.V. Monakhov, B.G. Svensson, M.K. Linnarsson, A. La Magna, M. Italia, V. Privitera, G. Fortunato, M. Cuscuna, L. Mariucci, Appl. Phys. Lett. 87 (2005) 192109.
[147] J. Venturini, M. Hernandez, G. Kerrien, C. Laviron, D. Camel, J.L. Santailler, T. Sarnet, J. Boulmer, Thin Solid Films 453–454 (2004) 145–149.
[148] N. Bernstein, M.J. Aziz, E. Kaxiras, Phys. Rev. B 61 (2000) 6696.
[149] K. Gärtner, B. Weber, Nucl. Instrum. Methods Phys. Res. B 202 (2003) 255–260.
[150] B.A. Gillespie, H.N.G. Wadley, J. Cryst. Growth 311 (2009) 3195–3203.
[151] N.G. Rudawski, K.S. Jones, R. Gwilliam, Mater. Sci. Eng. R 61 (2008) 40–58.
[152] N.G. Rudawski, K.S. Jones, S. Morarka, M.E. Law, R.G. Elliman, J. Appl. Phys. 105 (2009) 081101–081120.
[153] J. Jie, W. Zhang, K. Peng, G. Yuan, C.S. Lee, S.T. Lee, Adv. Funct. Mater. 18 (2008) 3251–3257.
[154] Y. Cui, Z. Zhong, D. Wang, W.U. Wang, C.M. Lieber, Nano Lett. 3 (2003) 149–152.
[155] R. Vaidyanathan, E.G. Seebauer, H. Graoui, M.A. Foad, Appl. Phys. Lett. 89 (2006) 152114.
[156] S.H. Yeong, M.P. Srinivasan, B. Colombeau, L. Chan, R. Akkipeddi, C.T.M. Kwok, R. Vaidyanathan, E.G. Seebauer, Appl. Phys. Lett. 91 (2007) 102112.
[157] X. Zhang, M. Yu, C.T.M. Kwok, R. Vaidyanathan, R.D. Braatz, E.G. Seebauer, Phys. Rev. B 74 (2006) 235301.
[158] K. Dev, E.G. Seebauer, Surf. Sci. 550 (2004) 185–191.
[159] M.Y.L. Jung, R. Gunawan, R.D. Braatz, E.G. Seebauer, J. Appl. Phys. 95 (2004) 1134–1140.
[160] K.A. Schultz, E.G. Seebauer, J. Chem. Phys. 97 (1992) 6958–6967.
[161] M.Y.L. Jung, R. Vaidyanathan, C.T.M. Kwok, E. G. Seebauer (in preparation).
[162] R. Vaidyanathan, New forms of defect engineering in silicon and metal oxide semiconductors, Ph.D. thesis, University of Illinois at Urbana-Champaign, 2007.
[163] M.Y.L. Jung, New surface and optically stimulated physics for modeling diffusion in silicon, Ph.D. thesis, University of Illinois at Urbana-Champaign, 2003.
[164] M.Y.L. Jung, E.G. Seebauer, Extended Abstracts of the 4th International Workshop on Junction Technology, IEEE, Shanghai, 2004, pp. 87–89.
[165] E.G. Seebauer, in: Proceedings of the 8th International Conference on Solid-State and Integrated Circuits Technology, IEEE, Shanghai, 2007, pp. 450–453.
[166] R. Vaidyanathan, M.Y.L. Jung, R.D. Braatz, E.G. Seebauer, AIChE J. 52 (2006) 366–370.
[167] W. Shockley, J.W.T. Read, Phys. Rev. 87 (1952) 823–842.
[168] J.G. Simmons, G.W. Taylor, Phys. Rev. B (Solid State) 4 (1971) 502–511.
[169] R. Vaidyanathan, S. Felch, H. Graoui, M.A. Foad, E.G. Seebauer (in preparation).
[170] Y. Kondratenko, Ph.D. thesis, University of Illinois at Urbana-Champaign, 2009.
[171] C. Claeys, E. Simoen, K. Opsomer, D.P. Brunco, M. Meuris, Mater. Sci. Eng. B 154–155 (2008) 49–55.
[172] G. Impellizzeri, S. Mirabella, E. Bruno, A.M. Piro, M.G. Grimaldi, J. Appl. Phys. 105 (2009) 063533.
[173] A. Satta, A. D'Amore, E. Simoen, W. Anwand, W. Skorupa, T. Clarysse, B. Van Daele, T. Janssens, Nucl. Instrum. Methods Phys. Res. B 257 (2007) 157–160.
[174] S. Heo, S. Baek, D. Lee, M. Hasan, H. Jung, J. Lee, H. Hwang, Electrochem. Solid-State Lett. 9 (2006) 136–137.
[175] J. Huang, N. Wu, Q. Zhang, C. Zhu, A.A.O. Tay, G. Chen, M. Hong, Appl. Phys. Lett. 87 (2005) 173507.
[176] E. Simoen, A. Satta, A. D'Amore, T. Janssens, T. Clarysse, K. Martens, B. De Jaeger, A. Benedetti, I. Hoflijk, B. Brijs, M. Meuris, W. Vandervorst, Mater. Sci. Semicond. Process. 9 (2006) 634–639.
[177] W.C. Dunlap Jr., Phys. Rev. 94 (1954) 1531–1540.
[178] S. Uppal, A.F.W. Willoughby, J.M. Bonar, A.G.R. Evans, N.E.B. Cowern, R. Morris, M.G. Dowsett, J. Appl. Phys. 90 (2001) 4293–4295.
[179] A. Satta, E. Simoen, T. Clarysse, T. Janssens, A. Benedetti, B. De Jaeger, M. Meuris, W. Vandervorst, Appl. Phys. Lett. 87 (2005) 172109.
[180] A. Axmann, M. Schulz, C.R. Fritzsche, Appl. Phys. 12 (1977) 173–178.
[181] A. Satta, T. Janssens, T. Clarysse, E. Simoen, M. Meuris, A. Benedetti, I. Hoflijk, B. De Jaeger, C. Demeurisse, W. Vandervorst, J. Vac. Sci. Technol. B 24 (2006) 494–498.
[182] J.F. Geisz, S. Kurtz, M.W. Wanlass, J.S. Ward, A. Duda, D.J. Friedman, J.M. Olson, W.E. McMahon, T.E. Moriarty, J.T. Kiehl, Appl. Phys. Lett. 91 (2007) 023502.
[183] R.R. King, D.C. Law, K.M. Edmondson, C.M. Fetzer, G.S. Kinsey, H. Yoon, R.A. Sherif, N.H. Karam, Appl. Phys. Lett. 90 (2007) 183516.
[184] F.D. Newman, M.A. Stan, S.L. Murray, C.S. Murray, J. Cryst. Growth 272 (2004) 650–657.
[185] B. Beaumont, P. Vennéguès, P. Gibart, Phys. Status Solidi B 227 (2001) 1–43.
[186] A. Sakai, H. Sunakawa, A. Usui, Appl. Phys. Lett. 73 (1998) 481–483.
[187] A.P. Edwards, J.A. Mittereder, S.C. Binari, D.S. Katzer, D.F. Storm, J.A. Roussos, IEEE Electron Device Lett. 26 (2005) 225–227.
[188] H. Hasegawa, T. Inagaki, S. Ootomo, T. Hashizume, J. Vac. Sci. Technol. B 21 (2003) 1844–1855.
[189] G. Verzellesi, A. Mazzanti, A.F. Basile, A. Boni, E. Zanoni, C. Canali, IEEE Trans. Electron Devices 50 (2003) 1733–1740.
[190] R. Yeats, D.C. D'Avanzo, K. Chan, N. Fernandez, T.W. Taylor, C. Vogel, Technical Digest – International Electron Devices Meeting, IEEE, 1988, pp. 842–845.
[191] S.C. Binari, P.B. Klein, T.E. Kazior, Proc. IEEE 90 (2002) 1048–1058.
[192] T. Hashizume, J. Kotani, H. Hasegawa, Appl. Phys. Lett. 84 (2004) 4884–4886.
[193] W. Saito, M. Kuraguchi, Y. Takada, K. Tsuda, I. Omura, T. Ogura, IEEE Trans. Electron Devices 52 (2005) 159–164.
[194] K. Keem, J. Kang, C. Yoon, D.Y. Jeong, B.M. Moon, S. Kim, Jpn. J. Appl. Phys. 46 (2007) 6230–6232.
[195] P.C. Chang, Z. Fan, C.J. Chien, D. Stichtenoth, C. Ronning, J.G. Lu, Appl. Phys. Lett. 89 (2006) 133113.
[196] C. Lao, Y. Li, C.P. Wong, Z.L. Wang, Nano Lett. 7 (2007) 1323–1328.
[197] C.S. Enache, J. Schoonman, R. Van De Krol, J. Electroceram. 13 (2004) 177–182.
[198] H. Matsui, H. Tabata, N. Hasuike, H. Harima, B. Mizobuchi, J. Appl. Phys. 97 (2005) 1–8.
[199] C.S. Enache, J. Schoonman, R.V. Krol, J. Electroceram. 13 (2004) 177–182.
[200] H. Matsui, H. Tabata, N. Hasuike, H. Harima, B. Mizobuchi, J. Appl. Phys. 97 (2005) 123511.
[201] E.-J. Lee, S.-I. Pyun, J. Appl. Electrochem. 22 (1992) 156–160.
[202] E. Comini, C. Baratto, G. Faglia, M. Ferroni, A. Vomiero, G. Sberveglieri, Prog. Mater. Sci. 54 (2009) 1–67.
[203] X.J. Huang, Y.K. Choi, Sens. Actuators B 122 (2007) 659–671.
[204] A. Kolmakov, M. Moskovits, Annu. Rev. Mater. Res. 34 (2004) 151–180.
[205] G. Shen, P.C. Chen, K. Ryu, C. Zhou, J. Mater. Chem. 19 (2009) 828–839.
[206] E. Comini, Anal. Chim. Acta 568 (2006) 28–40.
[207] N. Yamazoe, Sens. Actuators B 5 (1991) 7–19.
[208] Z. Fan, J.G. Lu, Appl. Phys. Lett. 86 (2005) 123510.
[209] M.W. Ahn, K.S. Park, J.H. Heo, J.G. Park, D.W. Kim, K.J. Choi, J.H. Lee, S.H. Hong, Appl. Phys. Lett. 93 (2008) 263103.
[210] B. Lei, C. Li, D. Zhang, T. Tang, C. Zhou, Appl. Phys. A 79 (2004) 439–442.
[211] P. Nguyen, H.T. Ng, J. Kong, A.M. Cassell, R. Quinn, J. Li, J. Han, M. McNeil, M. Meyyappan, Nano Lett. 3 (2003) 925–928.
[212] N. Wang, Y. Cai, R.Q. Zhang, Mater. Sci. Eng. R 60 (2008) 1–51.
[213] S. Geburt, D. Stichtenoth, S. Muller, W. Dewald, C. Ronning, J. Wang, Y. Jiao, Y.Y. Rao, S.K. Hark, Q. Li, J. Nanosci. Nanotechnol. 8 (2008) 244–251.
[214] B. Guo, A. Bermak, P.C.H. Chan, G.Z. Yan, IEEE Sens. J. 8 (2008) 1397–1398.
[215] L. Liao, H.B. Lu, J.C. Li, C. Liu, D.J. Fu, Y.L. Liu, Appl. Phys. Lett. 91 (2007) 173110.
[216] S. Lettieri, A. Setaro, C. Baratto, E. Comini, G. Faglia, G. Sberveglieri, P. Maddalena, New J. Phys. 10 (2008) 043013.
[217] C. Baratto, S. Todros, G. Faglia, E. Comini, G. Sberveglieri, S. Lettieri, L. Santamaria, P. Maddalena, Sens. Actuators B 140 (2009) 461–466.
[218] G. Faglia, C. Baratto, G. Sberveglieri, M. Zha, A. Zappettini, Appl. Phys. Lett. 86 (2005) 011923.
[219] E. Comini, C. Baratto, G. Faglia, M. Ferroni, G. Sberveglieri, J. Phys. D: Appl. Phys. 40 (2007) 7255–7259.
[220] A. Fujishima, K. Hashimoto, T. Watanabe, TiO_2 Photocatalysis: Fundamentals and Applications, Bkc, Tokyo, 1999.
[221] A. Fujishima, K. Honda, Nature 238 (1972) 37–38.
[222] A. Fujishima, T.N. Rao, D.A. Tryk, J. Photochem. Photobiol. C 1 (2000) 1–21.
[223] D. Li, H. Haneda, J. Photochem. Photobiol. A 155 (2003) 171–178.
[224] S. Sakthivel, B. Neppolian, M.V. Shankar, B. Arabindoo, M. Palanichamy, V. Murugesan, Sol. Energy Mater. Sol. Cells 77 (2003) 65–82.
[225] S.K. Kansal, M. Singh, D. Sud, J. Hazard. Mater. 141 (2007) 581–590.
[226] M. Miyauchi, A. Nakajima, T. Watanabe, K. Hashimoto, Chem. Mater. 14 (2002) 2812–2816.
[227] K.R. Reyes-Gil, E.A. Reyes-García, D. Raftery, J. Phys. Chem. C 111 (2007) 14579–14588.
[228] Y. Sun, C.J. Murphy, K.R. Reyes-Gil, E.A. Reyes-Garcia, J.P. Lilly, D. Raftery, Int. J. Hydrogen Energy 33 (2008) 5967–5974.
[229] C. Burda, Y. Lou, X. Chen, A.C.S. Samia, J. Stout, J.L. Gole, Nano Lett. 3 (2003) 1049–1051.
[230] W. Choi, A. Termin, M.R. Hoffmann, J. Phys. Chem. 98 (1994) 13669–13679.

[231] F. Gracia, J.P. Holgado, A. Caballero, A.R. Gonzalez-Elipe, J. Phys. Chem. B 108 (2004) 17466–17476.
[232] D. Wang, Y. Zou, S. Wen, D. Fan, Appl. Phys. Lett. 95 (2009), 012106–012108.
[233] J. Augustynski, Electrochim. Acta 38 (1993) 43–46.
[234] R. Asahi, T. Morikawa, T. Ohwaki, K. Aoki, Y. Taga, Science 293 (2001) 269–271.
[235] O. Diwald, T.L. Thompson, E.G. Goralski, S.D. Walck, J.T. Yates Jr., J. Phys. Chem. B 108 (2004) 52–57.
[236] A. Ghicov, J.M. Macak, H. Tsuchiya, J. Kunze, V. Haeublein, L. Frey, P. Schmuki, Nano Lett. 6 (2006) 1080–1082.
[237] J.L. Gole, J.D. Stout, C. Burda, Y. Lou, X. Chen, J. Phys. Chem. B 108 (2004) 1230–1240.
[238] H. Irie, Y. Watanabe, K. Hashimoto, J. Phys. Chem. B 107 (2003) 5483–5486.
[239] H. Wang, J.P. Lewis, J. Phys.: Condens. Matter. 18 (2006) 421–434.
[240] C. Di Valentin, G. Pacchioni, A. Selloni, Chem. Mater. 17 (2005) 6656–6665.
[241] S.U.M. Khan, M. Al-Shahry, W.B. Ingler Jr., Science 297 (2002) 2243–2245.
[242] J.H. Park, S. Kim, A.J. Bard, Nano Lett. 6 (2006) 24–28.
[243] H. Luo, T. Takata, Y. Lee, J. Zhao, K. Domen, Y. Yan, Chem. Mater. 16 (2004) 846–849.
[244] T. Ohno, T. Mitsui, M. Matsumura, Chem. Lett. 32 (2003) 364–365.
[245] J.C. Yu, W. Ho, J. Yu, H. Yip, K.W. Po, J. Zhao, Environ. Sci. Technol. 39 (2005) 1175–1179.
[246] M. Zheng, J. Wu, Appl. Surf. Sci. 255 (2009) 5656–5661.
[247] R.G. Breckenridge, W.R. Hosler, Phys. Rev. 91 (1953) 793–802.
[248] D.C. Cronemeyer, Phys. Rev. 113 (1959) 1222–1226.
[249] T. Ihara, M. Miyoshi, M. Ando, S. Sugihara, Y. Iriyama, J. Mater. Sci. 36 (2001) 4201–4207.
[250] I. Nakamura, N. Negishi, S. Kutsuna, T. Ihara, S. Sugihara, K. Takeuchi, J. Mol. Catal. A: Chem. 161 (2000) 205–212.
[251] P. Salvador, M.L.G. González, F. Muñoz, J. Phys. Chem. 96 (1992) 10349–10353.
[252] K. Takeuchi, I. Nakamura, O. Matsumoto, S. Sugihara, M. Ando, T. Ihara, Chem. Lett. (2000) 1354–1355.
[253] S. Baruah, S.S. Sinha, B. Ghosh, S.K. Pal, A.K. Raychaudhuri, J. Dutta, J. Appl. Phys. 105 (2009) 074308.
[254] H. Bracht, E.E. Haller, R. Clark-Phelps, Phys. Rev. Lett. 81 (1998) 393.
[255] A. Ural, P.B. Griffin, J.D. Plummer, Phys. Rev. Lett. 83 (1999) 3454.
[256] D. Eaglesham, Phys. World 8 (1995) 41–46.
[257] C.W.M. Castleton, A. Hoglund, S. Mirbt, Phys. Rev. B 73 (2006) 035215.
[258] C.W.M. Castleton, S. Mirbt, Phys. Rev. B 70 (2004) 195202.
[259] G. Makov, M.C. Payne, Phys. Rev. B 51 (1995) 4014.
[260] J. Lento, J.L. Mozos, R.M. Nieminen, J. Phys.: Condens. Matter. 14 (2002) 2637–2645.
[261] C.G. Van de Walle, J. Neugebauer, J. Appl. Phys. 95 (2004) 3851–3879.
[262] J.V. Beck, K.J. Arnold, Parameter Estimation in Engineering and Science, Wiley, New York, 1977.
[263] M.Y.L. Jung, R. Gunawan, R.D. Braatz, E.G. Seebauer, AIChE J. 50 (2004) 3248–3256.
[264] C.T.M. Kwok, K. Dev, R.D. Braatz, E.G. Seebauer, J. Appl. Phys. 98 (2005) 013524.
[265] M.Y.L. Jung, R. Gunawan, R.D. Braatz, E.G. Seebauer, J. Electrochem. Soc. 150 (2003) G838–G842.
[266] R. Gunawan, M.Y.L. Jung, E.G. Seebauer, R.D. Braatz, AIChE J. 49 (2003) 2114–2123.